Allosteric activation of T cell antigen receptor signalling by quaternary structure relaxation

Anna-Lisa Lanz[1,8,9], Giulia Masi[1,8,10], Nicla Porciello[1,8], André Cohnen[1,8,11], Deborah Cipria[1], Dheeraj Prakaash[2], Štefan Bálint[3], Roberto Raggiaschi[1], Donatella Galgano[1,12], David K. Cole[4,5], Marco Lepore[5], Omer Dushek[6], Michael L. Dustin[3], Mark S. P. Sansom[7*], Antreas C. Kalli[2,7*] and Oreste Acuto[1*]

[1]T cell signalling laboratory, Sir William Dunn School of Pathology, University of Oxford, Oxford, OX1 3RE, UK.

[2]Leeds Institute of Cardiovascular and Metabolic Medicine and Astbury Center for Structural Molecular Biology, University of Leeds, Leeds, LS2 9JT, UK.

[3]Kennedy Institute of Rheumatology, University of Oxford, Oxford, OX3 7FY, UK.

[4]Division of Infection & Immunity, Cardiff University, Cardiff, CF14 4XN, UK.

[5]Immunocore Ltd., Abingdon, OX14 4RY, UK.

[6] Sir William Dunn School of Pathology, University of Oxford, Oxford, OX1 3RE, UK.

[7]Department of Biochemistry, University of Oxford, Oxford, OX1 3QU, UK.

[8]The authors contributed equally.

*Corresponding authors: Oreste Acuto (oreste.acuto@path.ox.ac.uk), Mark S. P. Sansom (mark.sansom@bioch.ox.ac.uk), Antreas C. Kalli (A.Kalli@leeds.ac.uk).

Current addresses:

[9]Department of Pediatrics, Dr. von Hauner Children's Hospital, University Hospital, Ludwigs-Maximilians Universität, Munich, Germany.

[10]Enara Bio BioEscalator, Innovation Building, Oxford, OX3 7FZ, UK.

[11]Bayer AG, Müllerstrasse 178, 13353 Berlin, Germany.

[12]Center for Infectious Medicine, F59, Department of Medicine, Karolinska Institutet Karolinska University Hospital Huddinge, S-14186 Stockholm, Sweden.

Summary

The mechanism of T cell antigen receptor (TCR-CD3) signalling remains elusive. Here, we identified mutations in the transmembrane region of TCRβ or CD3ζ that augmented pMHC-induced signalling, not explainable by enhanced ligand binding, receptor diffusion, clustering or co-receptor function. Using a novel biochemical assay and molecular dynamics simulation, we found that the gain-of-function mutations modified transmembrane interactions that reduced TCRαβ cohesion with CD3ζ, suggesting that agonist pMHC binding may induce similar effects. Consistently, tetramer pMHC binding to TCR-CD3 reduced TCRαβ cohesion with CD3ζ, prior to CD3ζ phosphorylation. Moreover, we found that soluble monovalent pMHC alone induced signalling and reduced TCRαβ cohesion with CD3ζ in membrane-bound or solubilised TCR-CD3. Our data provide compelling evidence that pMHC binding suffices to activate allosteric changes propagating from TCRαβ to the CD3 subunits that reconfigure interchain transmembrane region interactions. This could modify the arrangement of TCR-CD3 boundary lipids to licence CD3ζ phosphorylation and initiate signal propagation.

Introduction

Signalling through the TCR-CD3 complex drives thymocyte maturation into immunocompetent T cells and T cell response to foreign antigens [1]. These processes initiate upon TCR-CD3 ligation by highly polymorphic major histocompatibility complex (MHC) proteins carrying short peptides (p) originated from the degradation of self and foreign proteins. TCR-CD3 allows T cells to respond with exceptional specificity and sensitivity [2] to membrane-bound pMHC ligands of a virtual continuum of weak K_d (0.1-250 μM) and $t_{1/2}$ of < 0.5 to a few seconds [3, 4, 5] and ligand-receptor interfaces of diverse shape and chemical reactivity. To accomplish this task, TCR-CD3 employs a clonally distributed αβ disulphide-linked dimer (TCR) with Ig-like variable domains, Vα and Vβ, containing the pMHC binding site composed of six loops homologous to antibody complementarity determining regions (CDRs) 1, 2 and 3 [6, 7]. Germline-encoded CDR1 and CDR2 have limited variability, while CDR3s are hypervariable. VαVβ is orientated diagonally relative to the long axis of the peptide-binding groove [6, 7], with CDR3s contacting mainly the peptide and CDR1s, and CDR2s contacting primarily the MHC [8, 9, 10]. Vα and Vβ are joined to Ig-like constant domains, Cα and Cβ, that are linked to transmembrane regions (TMRs) via a stalk connecting peptide (CP). pMHC binding is signalled intracellularly by four non-covalently associated subunits (γ, δ, ε and ζ), called CD3, organised into three dimers, γε, δε and ζζ, the latter disulphide-linked [11]. ε, γ and δ each exhibits an Ig-like extracellular domain (ECD) connected to their TMRs by short CPs, while ζ features a ≈ 10 residue-long ECD. A recent TCR-CD3 cryo-electron microscopy (EM) structure at 3.7 Å [12] generally reconciles with mutational and NMR studies [11, 13, 14] and reveals unsuspected features. The structure indicates that VαVβ projects forward while Cα interfaces with CD3δ ECD, Cβ interfaces with CD3γε and CD3δ ECDs, and CD3γ and CD3ε (of δε) ECDs contact each other. Whilst the TMRs of both ζζ subunits ($\zeta_1\zeta_2$) and of αβ interact with each other, δε is contacted by α and ζ_1, and γε is contacted by β and ζ_2. Further, the CPs of α, δ, and the ECD of ζ_1 are stabilised via polar interactions. This

highly interlaced structure suggests a mutualistic contribution of each dimer to the TCR-CD3 topology and cohesion. The intrinsically disordered intracellular tails of ε, γ, δ and ζ, invisible in the cryo-EM structure, contain immunoreceptor tyrosine-based activation motifs (ITAMs) that become phosphorylated by constitutively active Lck kinase [15] within ≤ 1 sec after pMHC binding [16, 17]. The CD3 tails are anchored to the plasma membrane (PM) via basic amino acid residues and ITAM tyrosines that interact with negatively charged lipids and hydrophobic interactions, respectively [18, 19], perhaps preventing ITAM phosphorylation of unliganded receptor by Lck. Early studies suggested that pMHC induces conformational changes that lead to the exposure of CD3 cytoplasmic tails [20]. However, crystallographic studies of pMHC bound to isolated TCRαβ ECD found considerable conformation changes in the CDRs [9, 10] but no unambiguous or consistent changes beyond the TCRαβ binding site. This led to propose signalling models independent of conformational changes or in which pMHC binding alone was insufficient to induce conformational changes of TCR-CD3. These models have suggested that pMHC-induced TCR-CD3 clustering [21, 22], co-receptors (CD8/CD4) recruitment [23] or segregation of the tyrosine phosphatase CD45 [24] initiated ITAMs phosphorylation and T cell activation. Alternatively, mechanosensing-based models have suggested that force generated by PM movements acts on pMHC-bound TCR-CD3 to induce conformational changes and signalling [25, 26]. Finally, it was proposed that clustering by pre-existing pMHC dimers drives conformational changes in CD3ε, but not directly in TCRαβ [20, 27]. Nevertheless, one crystal structure [28] and a fluorescence-based study [29] suggested that pMHC binding induced a conformational change in a Cα loop. Moreover, deuterium-exchange [30] and recent NMR investigations [31, 32] have indicated changes in conformational dynamics of pMHC-bound αβ ECD. These changes mapped to where Cα and Cβ interface with the ECD of the CD3 subunits [13, 14]. Although of great appeal, these studies do not rule in or out models proposed thus far; nor do they prove that allosteric effects propagate from αβ to the CD3 subunits for signalling to occur. To challenge this impasse, we conceived a genetic

perturbation analysis that should discriminate first between models requiring or not molecular flexibility. Towards this goal, we questioned the functional role of αβ TMR, as it is the physical connection between the module of the complex that binds pMHC and the intracellular milieu, where signals are delivered. If TMRs are exclusively required for TCR-CD3 solvation within the lipid bilayer and for quaternary structure topology, mutations should not change TCR-CD3 intrinsic capability to signal. In contrast, this could happen in mechanisms based on allosteric interaction or force. We gathered compelling genetic evidence for TMR mutations in TCRβ and CD3ζ that slightly modified the quaternary structure cohesion and augmented intrinsic signalling output. We also found that cohesion changes in TCR-CD3 quaternary structure and signal transduction were induced by soluble monomeric agonist pMHC and independently of co-receptor, clustering or force. We propose that allosteric activation of the T cell antigen receptor by pMHC binding is the prime mover of T cell activation.

Results

Gain-of-function mutations in β TMR

To question whether structural alterations in the TMR of the TCRαβ ligand-binding module affected signalling, we employed 1G4, an HLA-A2-restricted TCR specific for the 157-165 peptide from the NY-ESO-1 tumor antigen [33]. Most residues of TCRβ TMR were individually replaced by alanine or leucine and the corresponding mutants tested for reconstituting TCR-CD3 surface expression in the TCRβ-deficient 31.13 Jurkat cell line (J31.13) (Fig. **1A**). As reported earlier, βK287 mutation substantially reduced TCR-CD3 surface expression [34]. However, alanine substitution at βY281, βL285, βG286, βT289, βL290, βY291, βS296 and Leu at βA292 showed only a ≈ 20 % to 40 % decrease of surface expression. Next, the majority of mutants showing 0 % to 40 % reduction of surface expression were co-expressed together with WT 1G4 TCRα in J31.13 and Erk activation (pErk) was monitored after stimulation with 6V-HLA-A2 tetramer $(6V\text{-}A2)_4$ (Fig. **1B**). While no mutation significantly reduced Erk activation, both βA290 and βA291 significantly increased pErk. A gain-of-function was unexpected, even more so as βA290 and βA291 reduced TCR-CD3 surface expression (the data in Fig. **1B** are not normalised for TCR-CD3 surface expression).

βA291 heightens basal and ligand-induced signalling

To validate this apparently paradoxical observation, we focused on βA291 and modified the experimental set up to improve data robustness. Thus, α and β of 1G4 were expressed as a single self-cleavable polypeptide (Fig. **S1A**) from a doxycycline (dox)-inducible promoter in J76, a TCRαβ-deficient Jurkat cell line (Methods). J76 expressed maximum levels of surface TCR-CD3 after 16-18 h of dox treatment and were tested soon after to reduce potential risk of phenotypic drift of cells expressing 1G4 carrying βA291 (hereafter, referred to as 1G4-βA291). As in 31.13 cells, 1G4-βA291 expressed in J76 showed reduced surface expression (≈ 30 %) (cf. Fig. **1A** with Fig. **S1B**). However, in most experiments we lowered the dox

concentration when inducing 1G4-WT in order to reduce the difference in surface expression with 1G4-βA291 (to < 5%) (Fig. **S1C**). Moreover, in most flow-cytometry analyses, J76 expressing 1G4-WT or mutant were bar-coded by labelling with CellTrace™ violet, mixed before stimulation and analysed simultaneously. These stratagems considerably simplified and made more robust the computation of differences in signalling output between WT and mutant. Erk activation was retained as a sensitive and reliable read-out of TCR-CD3 signal transduction and propagation as it reports the occurrence of a cascade of very early and early signalling steps, including ITAM phosphorylation, ZAP-70 activation, LAT signalosome assembly and PLCγ1 activation that generates IP_3 (for intracellular [Ca^{2+}] increase) and DAG required for Ras activation by Ras-GRP [16]. Titration of $(6V\text{-}A2)_4$ showed a shift in pErk response by 1G4-βA291 towards higher sensitivity, but also revealed a significant higher Erk activation (Fig. **1C**). This was not due to a higher Erk activation ceiling in 1G4-βA291-expressing cells (Fig. **S1D**) nor to augmented binding of $(6V\text{-}A2)_4$ to 1G4-βA291 (Fig. **1D**, upper panel and lower panels), but it was consistent with the dose-response plot showing unchanged EC_{50} between 1G4-βA291 and 1G4-WT (Fig. **1C** and see Method for computation). The higher maximal response of 1G4-βA291 could be compatible with a faster proofreading rate (k_p) for a receptor operating in a kinetic proofreading regimen [35]. Indeed, fitting the data of Fig. **1C** into a minimal model of kinetic proofreading [36] showed the k_p for 1G4-βA291 being higher than 1G4-βWT (Fig. **S1E** and Methods), consistent with βA291 enhancing TCR-CD3 intrinsic signalling capability (i.e., enhancing ligand potency). Note that the gain-of-function was observed in J76 not expressing CD8 (Fig. **1C**), ruling out that the βA291 mutation enhanced TCR-CD3 interaction with co-receptor. Augmented signalling was also evident for ζ phosphorylation (pζ) (Figs. **1E** and **S1F**), the earliest intracellular signalling event. Remarkably, anti-CD3ε (UCHT1) Ab stimulation of 1G4-βA291 also heightened pζ (Fig. **S1G**), a triggering modality that by-passes pMHC binding, further supporting that βA291 enhanced TCR-CD3 signalling output. These data suggested that βA291 might increase

constitutive TCR-CD3 signalling that can be detected by measuring pζ in non-stimulated cells. Indeed, pζ was significantly higher basally in cells expressing 1G4-βA291 as compared to 1G4-WT (Figs. **1F** and **S1H**) and was specific as it disappeared, as expected, after treatment by A770041 [37] a potent and highly specific inhibitor of Lck (Fig. **S1I**). We then asked if βA291 increased signalling by influencing TCR-CD3 lateral diffusion and/or distribution. However, fluorescence recovery after photo-bleaching (FRAP) found no significant difference in the diffusion coefficient (D) between 1G4-βA291 and 1G4-WT (Fig. **1G**, left panel), which remained unchanged after A770041 treatment (Fig. **1G**, right panel). dSTORM super-resolution microscopy found no statistically significant difference in the cluster size distribution formed by 1G4-βA291 and 1G4-WT (histograms in Fig. **1H**). Although not statistically significant, the reproducible small increase of larger cluster frequency for 1G4-βA291 disappeared after A770041 treatment (cf. auto-correlation function plots in left and right panels of Fig. **1H**), indicating it to be secondary to 1G4-βA291 heightened basal signalling (Fig. **1F**), rather than βA291 causing it. Finally, we questioned the potential cause(s) of mildly reduced 1G4-βA291 surface expression. We excluded that βA291 reduced β protein expression (Fig. **S1J**) and considered that heightened basal signalling might decrease receptor surface expression by increasing its down-regulation rate. However, exposure to A770041 for several hours increased surface expression of both 1G4-βA291 and 1G4-WT in similar proportion (≈ 20 %) but did not significantly reduce their difference (Fig. **S1K**). These data led us to consider if βA291 modified the stability of TCR-CD3 quaternary structure that could reduce export to the PM due to negative triage by protein quality control systems [38].

βY291 contribution to TCR-CD3 quaternary structure cohesion

Non-ionic detergents used at high concentrations to quantitatively extract TCR-CD3 can dissociate TCRαβ from the CD3 modules [39]. Presumably, this can be attributed to the

substitution of natural boundary lipids by the detergent, with possible interference with TMR inter-helical interactions that are critical for TCR-CD3 quaternary structure cohesion [11, 12, 34]. However, 0.5 % of the non-ionic detergent n-Dodecyl-β-D-Maltopyranoside (DDM) allows quantitative extraction of stoichiometrically intact TCR-CD3 [40] (Fig. **S2A**). Thus, if βA291 altered TCRαβ cohesion with CD3 by unsettling TMR inter-helical interactions, 0.5 % DDM extraction may show lower recovery of intact 1G4-βA291 with respect to 1G4-WT. Figure **S2B** illustrates the conceptual and experimental set up of chemically probing TCR-CD3 cohesion by DDM that we named DDM Stability Assay (DSA) (see Methods for further details). Membrane solubilisation by 0.5 % DDM and pull-down (PD) of total β (mostly associated with α [41]) by the β-HA tag was followed by quantitative immunoblot (IB) for β (with anti-HA Ab) and for each CD3 subunit. Anti-HA IB identified three β isoforms (named β_1, β_2 and β_3, Fig. **2A**). β_3 was the endo-H-sensitive ER-resident β isoform (Fig. **S2C**) that is assembled with α, γε, δε but not with ζζ [41], as confirmed by β_3 being undetected in CD3ζ PD (Fig. **S2D**). β_1 and β_2 were both endo-H-resistant (Fig. **S2C**), though β_2 was the only β isoform associated with ζζ (Fig. **S2D**). Thus, to evaluate the effect of βA291 on TCR-CD3 complex cohesion we used the IB signals for β, ζζ and ε (including γε and δε). When ζ/β_2 was set equal to 1 for 1G4-WT (i.e., 100 % recovery of intact TCR-CD3), reduced cohesion between ζζ and αβ in 1G4-βA291 should result in $\zeta/\beta_2 < 1$ (Fig. **S2B**). The DSA showed that ζ/β_2 for 1G4-βA291 was 0.2, indicating only 20 % recovery of intact TCR-CD3 (or 80 % loss of ζζ recovery) after DDM solubilisation (Fig. **2A**). To determine the effect of βA291 on γε and δε cohesion with αβ, we used instead the sum of β_1, β_2 and β_3 (or total β (β_T) IB signals that represented cytoplasmic and PM αβ, most of which is associated with ε [41]. ε/β_T for 1G4-βA291 was ≈ 0.5 indicating ≈ 50 % reduced recovery of ε (Fig. **2A**). These ratios did not change after A770041 treatment during dox induction of αβ expression (Fig. **S2E**), excluding that reduced recovery concerned the pool of 1G4-βA291 with increased ζ basal phosphorylation (Fig. **1F**). The considerable reduction of ζ and ε recovery for 1G4-βA291

could not be the consequence of severance of αβ from the CD3 dimers at the PM, which is incompatible with PM expression [41] and even more so with increase of pMHC-induced signalling. Therefore, in the PM natural lipid environment βA291 only slightly perturbed TCR-CD3 quaternary structure cohesion that was instead severely corroded by DDM substituting for natural boundary lipids, provoking partial physical detachment of ζ and ε from αβ during the solubilisation. IB for γ and δ revealed that βA291 affected both γε and δε cohesion with the rest of the complex though asymmetrically, as it reduced γε and δε recovery of 40 % and 10 %, respectively (Figs. **2B** and **2C**). In the cryo-EM structure, βY291 (note that Dong *et al.* [12] refer to βY291 as βY292) contacts mostly γε and therefore βA291 can be expected to affect primarily the interaction between αβ and γε in accordance with the DSA. However, βY291 makes no contacts with ζζ and δε [12] (see MDS below). Therefore, the DSA revealed a more complex picture, with βA291 presumably affecting indirectly the interaction of both ζζ and δε with the rest of the complex. To further understand the structural role of βA291, we used the TMRs' atomic coordinates of the cryo-EM structure of the TCR-CD3 octamer (PDB: 6JXR) [12] to carry out all-atom molecular dynamics simulations (MDS) with βWT and βA291 in an asymmetric lipid bilayer, mimicking the lipid environment of TCR-CD3 (see Methods for details) and adding dynamical insight into TCR-CD3 cohesion. Simulations for 1250 ns confirmed considerable contacts of β WT with ε (of γε), γ, α and ζζ but not with δε (Figs. **2D** and **S2F**) and revealed one new contact of β with ζζ as well as significant reduction in six β contacts with ε (γε), five with γ and four with α (Fig. **S2F**). Specifically, during the simulations, significant contacts of βY291 with αN263, αT267, γL129, γG132, and εL145 were observed (Figs. **2D** right panel and **S2G**) and also with γV133 and γI136, though not considered significant on the normalised scale (Fig. **S2G**). No contacts of βY291 with ζζ were seen (Fig. **S2F**). Simulations of the TMR octamer carrying βA291 indicated new and augmented contacts of β with ε (γε) and γ (Fig. **S2H**). In addition, while βA291 still contacted

γL129, it completely lost interaction with γG132, γV133 and γI136 (Fig. **S2I**, middle panel). Likely, these changes were secondary to spatial re-adjustments due to the loss of the bulky tyrosine side chain. No contacts of βA291 with ζζ were observed. Overall, the simulations suggested that βA291 reshuffled contacts with γε, with the net effect of increasing local compaction (Fig. **S2J**), as also indicated by a stabilisation of their α-helices crossing angle (Fig. **S2K**). This result seemed to contradict the DSA data of βA291 severely affecting ζζ interaction with the rest of the complex. Although 1250 ns time-scale is relatively long for all-atom simulations of membrane proteins, it might be insufficient to capture re-adjustments of interchain contacts that possibly occur at larger time-scales. βA291 might affect the role of interfacial lipids in cementing α-helices interactions [42] that when challenged with DDM caused crumbling of TMRs' cohesion in the mutant, despite augmented compaction by βA291 elsewhere. However, reduced export to the PM was a good indicator that βA291 (and other β and ζTMR mutants, see below) promoted some instability of the complex, causing dynamical exposure of hydrophobic site and/or retention signals, detected and negatively triaged by protein quality control systems [38]. Comprehensively, these data suggested a positive correlation between reduced quaternary structure cohesion of TCR-CD3 and signal transduction activation.

Loosening ζ association enhances signalling

To corroborate this hypothesis, we investigated the phenotype of additional mutations in β and ζ TMRs. We found that similar to βA291, also βF291 and βL291 mildly reduced TCR-CD3 surface expression, despite no decrease in β expression (Fig. **3A**). Both mutations reduced interaction of β with ζ and ε (Fig. **3B**) and augmented pErk maximal response to $(6V\text{-}A2)_4$ (Fig. **3C** and **3D**), whose binding remained unchanged (Fig. **S3A**). These three readouts ranked according to: βL291 ≥ βA291 > βF291 > WT, presumably reflecting conservative or

non-conservative replacements, hence indicating a plausible direct correlation between increased quaternary structure loosening and heightened signalling. We then tested the effect of βA291 in 2H5, an HLA-A2-restricted TCR specific for the MART-1 tumour antigen (MART-1 $_{26-35}$ [43]). Similar to 1G4-βA291, 2H5-βA291 showed reduced surface expression (Fig. **3E**) and TCR-CD3 cohesion (Fig. **3F**) and augmented pErk for equal $(MART\text{-}1\text{-}A2)_4$ binding (Figs. **3G** and **S3B**). Conversely, mutation of β TMR residues not involved in critical contacts [12], such as βA293 and βA303, showed no significant change of 1G4 surface expression (Fig. **S3C**), TCR-CD3 cohesion (Figs. **S3D** and **S3E**) and no increase in $(6V\text{-}A2)_4$-induced pErk (Figs. **S3F** and **S3G**).

βY291 did not contact ζ, but its mutation augmented basal (Fig. **1F**) and ligand-induced ζ phosphorylation (Fig. **1E**) and signal propagation. This was reminiscent of allosteric interaction revealed by mutations [44, 45] - e.g., mutations at βY291 induced local re-adjustments but also distal functional effects, such as favouring exposure of ζ cytosolic tail to active-Lck. To investigate this possibility, we tested whether mutations in ζ TMR residues susceptible to loosen ζζ contacts with subunits other than αβ phenocopied mutations at βY291. TCR-CD3 cryo-EM structure and MDS indicated that ζ_1 and ζ_2 TMRs contacted only the N-terminal moiety of β TMR (Figs. **4A** and **S4A**) and α TMR throughout (Figs. **4B** and **S4B**). However, ζ_2 and ζ_1 contacted also γ (Figs. **4C** and **S4C**) and ε (of the δε) (Figs. **4D** and **S4D**), respectively. Specifically, MDS revealed that ζ_1I38 contacted two residues of ε (of δε) (Figs. **4D** and **S4E**, left panel) and ζ_2I41 contacted two residues of γ (Figs. **4C** and **S4F**, left panel), whereas ζ_2I38 and ζ_1I41 bulged toward the membrane lipids and made no contact with the complex. Thus, ζ_1I38 and ζ_2I41 were deemed capable of partially disturbing ζ_1 and ζ_2 interactions with ε (of δε) and γ, but not with αβ. To verify this prediction, 1250 ns all-atom simulations of TCR-CD3 octamer TMRs composed of ζ WT, ζA41 and ζA38 mutants were carried out. At the end of the simulations, alignment of snapshots of the mutated and WT TMRs showed distortion in the contacts of ζ_1 with δε (Fig. **4E**) and ζ_2 with γ (Fig. **4G**). As a

consequence, ζζ containing ζ_1A38 (3 out of 3 simulations) or ζ_2A41 (2 out of 3 simulations) increased fluctuation relative to αβ as compared to ζζ WT. This can be appreciated from the average spatial distribution plots of the Cα atoms of ζζ relative to the Cα atoms of αβ that show broader density for both mutants (Figs. **4F** and **4H**), though more pronounced for ζ_1A38. These results were indicative of ζA38 and ζA41 increasing ζζ flexibility relative to αβ. Both mutants maintained some ζζ contacts with the rest of the complex (Figs. **S4G** - **S4N**). These results prompted us to test if, similar to the βA291 mutations, also these ζ mutations showed reduced surface expression, complex cohesion by DSA and enhanced signalling. The data showed that ζA38 or ζA41 reduced 1G4 surface expression by 30 %, for similar ζ expression (Fig. **5A**). The DSA showed that ζA38 and ζA41 reduced ζ/β_2 ratio to 0.05 and 0.25 (95 % and 75 % loss of ζ recovery), respectively, without apparently affecting ε cohesion (Figs. **5B** and **S5A**). Thus, the DSA fully agreed with the atomistic simulation predictions, likely because the mutations involved residues making direct interactions of ζζ with the other helices. Simulations of larger time-scales may provide clearer insights into dynamic alterations of ζζ by βA291 that presumably first produced a direct effect on γε and later on ζζ. Importantly, similar to βA291, both ζ mutations conferred to 1G4 heightened pErk response to $(6V\text{-}A2)_4$, with a higher maximum compared to 1G4-WT (Figs. **5C** and **5D**) for equal $(6V\text{-}A2)_4$ binding (Figs. **S5B** and **S5C**). We concluded that the reduced quaternary structure cohesion between αβ and ζζ caused heightened signalling, rather than the mutations of βY291 *per se*. This strengthened the idea that reducing TCR-CD3 quaternary structure cohesion populated the active signalling state of TCR-CD3 -i.e., it lowered the activation energy between two presumably functional states: inactive and active, the latter initiating transmembrane signalling. These data made it highly unlikely that TCR-CD3 TMRs are just structural elements required for TCR-CD3 membrane solvation and architecture, as "rigid-body" signalling models would imply. Rather, by analogy with allosterically regulated proteins that can be switched on or off by mutations distal from their active site(s) [44, 45], and

considering recent NMR studies [14, 31, 32, 46], our data suggested that pMHC binding could activate an allosteric cascade that loosened TCR-CD3 cohesion including TMR interactions with ζζ TMRs serving as a second-to-last relay before licencing ζ ITAM phosphorylation. These considerations prompted us to investigate this hypothesis.

pMHC tetramer binding loosens αβ association with ζ

Conformational changes produced by pMHC binding may reduce contacts of CαCβ with δε and/or γε ECDs, eventually extending this effect to TMR contacts, including ζζ TMR and ultimately affect TCR-CD3 complex cohesion. If correct, the DSA should show reduced recovery of ζζ in ligand-engaged TCR-CD3. To test this idea, 1G4-WT-expressing J76 were briefly stimulated with $(9V\text{-}A2)_4$, tetramerised with His-tagged streptavidin [$(9V\text{-}A2)_4$-His] (Fig. **S6A** and Methods), ligand excess was removed and cells rapidly solubilised with 0.5 % DDM. Post-nuclear lysates were incubated with His-Cobalt beads for a quick capture of $(9V\text{-}A2)_4$-His-bound 1G4. This experimental setting failed to capture sufficient $(9V\text{-}A2)_4$-His-bound TCR-CD3, likely because the detergent interfered with the avidity gain due to tetramer-induced clustering in a membrane milieu, making the dissociation rate of individual 9V-A2 in the tetramer closer to that of a 9V-A2 monomer alone (i.e., a solution k_{off} of 0.33 s^{-1} at 25° C [3]). To overcome this limitation, we initially employed wtc51[47], a 1G4 variant harbouring four mutations in βCDR2 (Fig. **S6B**) that confer a 15 nM K_d for NY-ESO-$1_{157\text{-}165}$-HLA-A2 (k_{off} of 0.0013 s^{-1} at 25° C). Computational modelling showed that NY-ESO-$1_{157\text{-}165}$-HLA-A2 adopts a canonical orientation onto wtc51 VαVβ, almost indistinguishable from 1G4-WT (Fig. **S6B**). $(9V\text{-}A2)_4$-His induced robust wtc51-mediated Erk activation (Fig. **6A**, left panel) and allowed specific capture of engaged wtc51 (Fig. **6A**, middle panel, lanes 2 and 4), to be compared with unliganded wtc51 isolated by anti-HA β pull-down (Fig. **6A**, middle panel, lanes 1 and 3). β_2 was the only isoform bound to $(9V\text{-}A2)_4$-His (Fig. **6A**, middle panel, lanes 2 and 4), consistent with it being the only one associated to ζ and present at the cell surface

(Fig. **S2D**). Therefore, ζ/β_2 ratio was used to assess if pMHC binding had reduced cohesion of ζ within TCR-CD3 (Fig. **6A**, right panel). The data showed that ζ/β_2 in liganded wtc51 was 0.5 (Fig. **6A**, right panel), in agreement with pMHC binding causing TCR-CD3 relaxation. Reduced pMHC-induced TCR-CD3 cohesion was independent of ζ phosphorylation, as identical results were obtained after A770041 treatment (Fig. **6A** middle and right panels). Allosteric interaction typically occurs in the µs to few ms time-scale [45], similar to the time required by pMHC binding to induce conformational changes in Cβ loops [31]. Because pMHC binding dwell-times are of a much longer time-scale (e.g., hundreds of ms-to-sec), allosterically-induced conformational changes should be observable at non-physiological temperatures. Consistently, almost identical reduction of ζ/β_2 ratio was observed when $(9V\text{-}A2)_4$ was reacted with cells at 0 ^{o}C (Fig. **6B** middle and right panels). To exclude that our observations were biased by the particular mutations introduced in βCDR2 and/or by the non-physiological affinity of wtc51, we used QM-α TCR, a 1G4 variant carrying mutations in αCDR2, βCDR2 and βCDR3 (Fig. **S6B**) [47], which confer a 140 nM K_d (k_{off}, 0.015 sec^{-1} at 25° C) for NY-ESO-$1_{157\text{-}165}$-HLA-A2 [47], within the physiological range of TCR-pMHC binding affinity [48]. Modelling showed that the canonical orientation of QM-α and 1G4-WT onto NY-ESO-$1_{157\text{-}165}$-HLA-A2 were superimposable (Fig. **S6B**). Figure **6C** showed that binding of $(9V\text{-}A2)_4$-His to QM-α induced Erk activation (Fig. **6C**, left panel) and reduced ζ/β_2 ratio (40 %), which remained unchanged after A770041 treatment (Fig. **S6C**). These observations were extended to 868, a TCR isolated from an HIV elite controller [49]. 868 recognises a spontaneously mutated HIV p17 Gag-derived peptide SLYNTIATL (6I) presented by HLA-A2, with a K_d of 50 nM at 37 ^{o}C (k_{off}, 0.0013 at 4° C [4]). Being a natural TCR directed at a viral antigen, 868 was ideal to validate the data obtained with *in vitro*-modified TCRs against a tumour antigen. Binding of tetramerised ligand $(6I\text{-}A2)_4$-His stimulated strong Erk activation (Fig. **6D**, left panel) and weakened 868 quaternary structure cohesion, as shown by the reduced ζ/β_2 ratio (Fig. **6D**, middle and right panels). The same structural changes in three different TCRs

cannot be a coincidence but the consequence of the same effect, that is, ligand-induced conformational change propagating through the entire TCR-CD3 complex and reaching the TMRs. Reduced ζ cohesion was also observed in wtc51 when expressed in primary human T cells stimulated with $(9V\text{-}A2)_4$-His (Fig. **6E**), excluding non-physiological behaviour of TCR-CD3 in the PM of Jurkat cells. To date, it remains unclear whether anti-CD3ε Abs used in clinical settings activate TCR-CD3 by mechanisms distinct from that of pMHC. To address this question, we slightly modified the DSA (Methods). We employed mono-biotinylated Fab' of UCHT1 anti-CD3ε as a proxy for minimally- or non-stimulated receptor and mono-biotinylated UCHT1 Ab to stimulate and capture TCR-CD3 with streptavidin for IB analysis. Since TCR-CD3 was captured via CD3ε, β/ε and ζ/ε ratios were used to assess TCR-CD3 cohesion. We found that UCHT1 Ab binding reduced β/ε and ζ/ε ratios, hence the cohesion of ε with β but less so with ζ (Fig. **6F**). Similar observations were made if cells were pre-treated with A770041 (Figs. **6G** and **S6D**) or reacted with UCHT1 at 0 °C (Figs. **6H** and **S6E**). Taken together, these observations and the TMR mutant phenotype strongly suggested that TCR-CD3 signals intracellularly by an allosteric interaction propagating from the αβ binding site to the CD3 subunits.

Monovalent pMHC in solution triggers TCR-CD3 untying and intracellular signalling

pMHC tetramers induced conformational change and signalling without applying force. However, pMHC tetramers necessarily induced fast TCR-CD3 clustering and therefore cannot allow to discern if receptor aggregation was responsible for allosteric activation, as previously suggested [27]. We therefore reacted wtc51-expressing J76 with biotinylated soluble monovalent (sm)-9V-A2 (Fig. **7A**), controlled just before use for being monodispersed by size-exclusion chromatography (SEC) (Fig. **S7B**). Following DDM solubilisation, sm-9V-A2-bound TCR-CD3 was captured by His-Streptavidin/His-Cobalt beads (Fig. **S7A**) and ζ recovery examined. The data showed that ζ/β_2 ratio was considerably

reduced in sm-9V-A2-bound vs. unbound wtc51 and was unaffected by A770041 treatment (Fig. **7A**, IBs and histograms) or by the absence of CD8 co-receptor (Fig. **7B**). To definitively exclude potential sm-pMHC cross-linking after solubilisation by streptavidin used for capturing ligand-bound TCR-CD3, we used instead an Avidin monomer (mAv). However, this condition did not change the result (Fig. **S7D**). Similar ζ/β_2 reduction was observed for 868 TCR reacted with sm-6I-A2 (Figs. **7C**, IBs and histograms and **S7C**). Figure **7E** (IBs and histograms) shows that sm-9V-A2 reduced ζ recovery also in wtc51 expressed in primary T cells, excluding a bias of Jurkat cell PM. A stringent test for TCR-CD3 allosteric regulation was to assess whether sm-pMHC promotes quaternary structure untying after solubilisation. Figure **7F** shows that sm-9V-A2 added to wtc51 after cell solubilisation with 0.5 % DDM considerably reduced ζ/β_2 ratio. Thus, the allosteric mechanism that loosens TCR-CD3 quaternary structure largely relies on protein-protein interactions. Since it occurs also in isolated TCR-CD3, it strengthens the idea that pMHC-induced quaternary structure untying is independent of force, clustering and co-receptor. If the conformational change induced by sm-pMHC was functionally relevant, it should also induce intracellular signalling. Previous work could not demonstrate that binding of sm-pMHC in solution elicited $[Ca^{2+}]_i$ increase unless co-receptor was expressed [23]. However, we found that sm-9V-A2, rigorously controlled for being mono-dispersed (Fig. **S7B**), did induce robust pErk in both CD8-efficient (Fig. **7A**) and CD8-deficient (Fig. **7B**) J76 cells expressing wtc51, that was abolished by A770041 (Fig. **7A**). Erk activation by sm-9V-A2 was dose-dependent (Fig. **S7E**), with as little as 3 nM inducing 50 % of the maximum and occurred at 2 min after sm-9V-A2 addition (Fig. **S7F**), similar to $(9V\text{-}A2)_4$ stimulation of 1G4-WT [50]. We obtained similar data with 868 and in presence or absence of CD8 co-receptor (Figs. **7C**, **7D** and **S7C**). We did not detect non-specific adsorption of sm-pMHC onto J76 cell membrane during the stimulation assay even at the highest sm-9V-A2 concentration (Fig. **S7G**), excluding that quaternary structure untying and signalling were the consequence of surface cell-to-cell ligand cross-presentation

rather than stimulation by the soluble ligand. Multiple reasons can explain why our data apparently contradict previous observations. First and foremost, we used receptor of reduced k_{off} (higher-range of affinity) for pMHC. sm-pMHC ligands of low-medium affinity range (μM) can be expected to induce low/non-sustained $[Ca^{2+}]_i$ increase, whose robust ramp-up requires a complex cascade of additional events [51, 52], including co-receptor [23, 27]. Also, sm-pMHC engages TCR-CD3 without immediately clustering it, contrary to pMHC tetramers that provide this critical signalling-reinforcing effect (see Discussion). Moreover, membrane-tethered pMHC has lower degree of freedom than soluble pMHC, a property that sensibly increases pMHC on-rate [53, 54]. Comprehensively, our genetic, biochemical, MDS and functional data constitute substantial evidence that TCR-CD3 is a genuine allosteric device. We name this model "TCR-CD3 allosteric relaxation" (Fig. **S7H**) as a mechanism sufficient to incite initial T cell activation solely by pMHC binding.

Discussion

Allostery governs signal transduction of many membrane receptors [44]. However, this hard-wired, tuneable and fast interaction mode exploiting protein conformational flexibility has not gained sufficient traction for the elucidation of TCR-CD3 signalling mechanism [55]. To gather insight into TCR-CD3 signalling mode, we used a genetic perturbation approach and uncovered a previously unnoticed allosteric property of the entire TCR-CD3 complex. We found that TMR mutations that loosened cohesion between TCRαβ and CD3 populated TCR-CD3 activated state and increased agonist's potency. This gain-of-function phenotype mimicked pMHC agonist binding that also reduced cohesion between TCRαβ and CD3, independently of CD3 ITAM phosphorylation. These convergent results suggested that weakening of TCR-CD3 TMR contacts is a key step in an allosteric mechanism initiated by pMHC binding [56] and culminating in ITAM phosphorylation. We favour the idea that conformational changes occurring at the pMHC binding site propagate to CαCβ ECDs, where they contact the CD3 subunits as indicated by several investigations [29, 31, 32, 57]. The ECDs and TMRs of TCRαβ, CD3δε and CD3γε show extended intra-dimer interface, yet less so between dimers [12], suggesting that each dimer is a relatively compact module but retains flexibility vis-à-vis the other dimeric modules. Moreover, CD3δε and CD3γε interact much more with TCRαβ than with each other. It is therefore conceivable that pMHC binding induces reshuffling of ECD contacts that hold together TCRαβ, CD3δε and CD3γε, making the latter two acquire a higher degree of freedom vis-à-vis TCRαβ. This spatial dislocation may result in slight rotations and/or translations of CD3δε and/or CD3γε vis-à-vis TCRαβ. The mechanical rigidity conferred to the CPs of ε, δ and γ by the Cys-Cys loop [41] could transmit these movements to the respective TMRs, resulting in local rearrangements of helix-helix packing (similar to TMR mutations analysed here) and of interfacial lipids [42] (Fig. **S7H**). Consistently, mutations of ε Cys-Cys loop affect TCR-CD3 signalling [41, 58]. The relaxed

quaternary structure of ligand-activated TCR-CD3 could also reduce contacts between the dimers' TMRs, making ζζ (the most loosely attached dimer) prone to lose contacts with the rest of the complex further eroded by detergent extraction as we show here. As our data suggest, TMR quaternary structure relaxation activated by pMHC (and anti-CD3 Ab) or by TMR mutations promotes ITAM accessibility by active-Lck [15]. We think it is unlikely that TMRs reconfiguration is mechanically transmitted to the CD3 intracellular tails, as the membrane-juxtaposed segments of all CD3 subunits are intrinsically disordered, hence they lack mechanical rigidity. We suggest instead that the subtle untying of TMRs may indirectly reduce the grip of CD3 intracellular tails anchorage to the inner leaflet of the PM and ITAM tyrosine hiding [19], normally secured from phosphorylation by constitutively active-Lck in unliganded TCR-CD3 (Fig. **S7H**). Phosphatidylserine (PS) [19] and PIP2 [59] are thought to keep the CD3 tails retracted onto the PM. An attractive possibility is that local TMR octamer rearrangement permits fast exchange of PIP2 and PS with neutral lipids that may reduce CD3ζ and ε tails interaction with the lipid bilayer (Fig. **S7H**), gradually augmenting the exposure of ITAM tyrosines to active-Lck. Changes in cholesterol interacting with TMR helices [56, 60] and/or with the tyrosines of the ITAMs might also help regulate this mechanism. Agonist anti-CD3ε mAb produced similar gain-of-function of TMR mutants and quaternary structure untying, in agreement with CD3ε ECD lying on the conformational trajectory activated by pMHC binding.

A key finding of our investigation is the formal evidence that binding of soluble monovalent and mono-dispersed pMHC (sm-pMHC) alone to membrane-bound or detergent-solubilised TCR-CD3 suffices to induce TCR-CD3 quaternary structure relaxation and induce signal transduction. Stimulation of TCR-CD3 by sm-pMHC alone agrees with a genuine allosteric mechanism, as hinted by the genetic perturbation analysis, much like classic membrane receptors activated by soluble ligands. Allosteric activation occurred without either co-receptor or TCR-CD3 clustering or force, making extrinsic energy source, such as actomyosin-

induced membrane movements invoked by mechanosensing [25, 61] or some receptor clustering models [62], dispensable for signalling. In order to analyse biochemically the status of pMHC-engaged (monomer or tetramer) vs. free TCR-CD3, 1G4 TCR binding to 9V-A2 with a K_d of ≈ 10 μM was insufficient. However, we succeeded in doing so by using 1G4 variants wtc51 and QM-α capable of binding 9V-A2 with a K_d of 0.02 μM and 0.140 μM, respectively, the latter within the physiological K_d range for pMHC agonists [3, 5, 48]. A third example was 868, a CTL-derived anti-HIV TCR isolated from an elite controller, whose K_d of 0.11 μM towards the p17 Gag-derived epitope was raised to 0.05 μM by a naturally occurring mutation in the same epitope [4]. All these three TCRs engaged by sm-pMHC showed ligand-induced quaternary structure loosening and intracellular signalling. We think it is unlikely that the increased affinity for pMHC confers to TCR-CD3 an allosterically regulated signalling while lower affinities do not. Indeed, allosteric changes in TCRαβ have been also demonstrated using NMR with pMHC of μM K_d [29, 31, 32, 57].

It has been long held that pMHC monomer alone cannot trigger TCR signalling, a claim based on early work that could not detect $[Ca^{2+}]_i$ increase with sm-pMHC, unless CD8 was co-engaged [23]. Others also have dismissed that pMHC monomer stimulates TCR-CD3 [63]. This apparent conflict with our data can be reconciled by considering differences in sensitivity of the signalling outputs measured (i.e., $[Ca^{2+}]_i$ vs. pErk) and the contribution to pMHC binding on-rate (excluding co-receptors contribution). Membrane-tethered pMHC shows considerably increased k_{on} compared to sm-pMHC and little or no effect on the k_{off} [53, 54], suggesting that membrane-tethered pMHC agonists should in general manifest stronger signalling than when in solution. Thus, for instance $[Ca^{2+}]_i$ rise of high amplitude and duration requires sustained TCRαβ engagement [51, 52], likely achieved by higher lateral ordering of cell-surface and signalling complexes in micro-clusters and immunological synapse (IS) [64]. This complex combination of events (e.g., clustering or co-receptor intervention) that sets in motion full T cell activation, may not be required for the initiation

of TCR-CD3 signal transduction. In contrast, sustained signalling (and full cell activation) cannot be achieved by sm-pMHC alone.

Mechanical forces play multiple roles in T cell activation at the molecular and cellular levels [65]. TCR-pMHC interaction life-time can be prolonged (i.e., reduced k_{off}) when subjected to ≈ 10 - 20 pN pulling force, which means that "catch-bond" can be formed [65]. However, this takes several seconds [26] and is not required to trigger TCR signalling [66]. Instead, pMHC-induced signal transduction without active mechanical force is consistent with allosteric interactions propagating in µs to ms [31, 32, 67]. This is much faster than effects induced by mechanical force (pulling/pushing) generated by membrane fluctuations and/or dedicated actin protrusions occurring in seconds.

Changes in conformational dynamics can have long-range consequences of functional relevance, a mechanism known as dynamic allostery [68], which relies on changes in conformational entropy only. Conformational entropy cannot be frequently observed in a protein's crystalline state that represents mostly energy minima, unlikely to capture a protein higher-energy (activated) state. However, NMR can correlate very fast local conformational changes (ps, ns) occurring at distant sites over time scales of µs to ms, compatible with allosteric regulation [67]. Dynamic allostery may therefore apply to TCRαβ, as pMHC binding induces changes in conformational dynamics at distal H3, H4 helices and FG loop of Cβ and Cα AB loop [29, 31, 32, 57], the latter having been captured only in a single crystal structure [28] of many solved to date (http://atlas.wenglab.org/web/index.php).

Our data and a closer look at previous works should help reconcile controversies about TCR-CD3 signalling mechanism. Thus, pMHC co-engagement by TCR and co-receptor has been found to be conditional on initial TCR-CD3 signalling [69, 70] and catch-bonding was contrasted by inhibiting Lck [66]. We found that enhanced basal signalling by 1G4-βA291 induced weak but detectable clustering that was erased by Lck inhibition. These data suggest that all these events are instigated by an initial one that we propose to be allosteric activation induced by

solely pMHC binding. Thus, co-receptor engagement, receptor clustering, shielding from PTPs and actomyosin-driven mechanical force (consequent catch-bonding) may constitute mechanisms that stabilise and potentiate initial allosterically-induced signalling. They may help reduce physical and chemical noise during receptor signalling, augmenting and stabilising signals of narrow amplitude and duration initiated by sparse engagement of pMHC monomers [71].

The fast time-scale by which allosteric interaction operates should ensure that ITAMs' exposure to active-Lck can rely on pMHC binding dwell-time compatible with both very weak (self) and agonist ligands (e.g., hundreds of ms to sec). However, allosteric activation for receptors that recognise multiple ligands raises the possibility of "biased agonism" [72, 73, 74] whereby different ligand-induced conformational changes and/or ligand-binding kinetics correlate with distinct functional outputs. In principle, allosteric interaction activated by different TCR$\alpha\beta$ CDR loop conformational changes upon canonical orientations over pMHC might follow different conformational trajectories propagating along TCR-CD3. In this case, ligand potency may result from both binding kinetics and variable conformational trajectories. Alternatively, TCR-CD3 structural dynamics might have evolved to "normalise" propagation of diverse conformational changes to generate seemingly equivalent allosteric changes (e.g., for ECDs, TMRs and CD3 tails), making ligand binding kinetics the unique factor governing ligand potency. Future studies on TCR-CD3 using native nanodiscs, cryo-EM, MDS and genetic perturbation should help to further clarify these questions. We anticipate that the novel data for TCR-CD3 signalling reported here should spark interest for innovative strategies to harness TCR-CD3 signalling for immunotherapy.

Methods

Please refer to Supplementary Information for a detailed description of all experimental procedures used in this investigation.

Bibliography

1. Stritesky, G.L., Jameson, S.C. & Hogquist, K.A. Selection of self-reactive T cells in the thymus. *Annual review of immunology* **30**, 95-114 (2012).

2. Davis, M.M. *et al.* T cells as a self-referential, sensory organ. *Annual review of immunology* **25**, 681-695 (2007).

3. Aleksic, M. *et al.* Dependence of T cell antigen recognition on T cell receptor-peptide MHC confinement time. *Immunity* **32**, 163-174 (2010).

4. Cole, D.K. *et al.* Dual Molecular Mechanisms Govern Escape at Immunodominant HLA A2-Restricted HIV Epitope. *Frontiers in immunology* **8**, 1503 (2017).

5. Stone, J.D., Chervin, A.S. & Kranz, D.M. T-cell receptor binding affinities and kinetics: impact on T-cell activity and specificity. *Immunology* **126**, 165-176 (2009).

6. Garboczi, D.N. *et al.* Structure of the complex between human T-cell receptor, viral peptide and HLA-A2. *Nature* **384**, 134-141 (1996).

7. Garcia, K.C. *et al.* An alphabeta T cell receptor structure at 2.5 A and its orientation in the TCR-MHC complex. *Science* **274**, 209-219 (1996).

8. Marrack, P., Scott-Browne, J.P., Dai, S., Gapin, L. & Kappler, J.W. Evolutionarily conserved amino acids that control TCR-MHC interaction. *Annual review of immunology* **26**, 171-203 (2008).

9. Baker, B.M., Scott, D.R., Blevins, S.J. & Hawse, W.F. Structural and dynamic control of T-cell receptor specificity, cross-reactivity, and binding mechanism. *Immunol Rev* **250**, 10-31 (2012).

10. Garcia, K.C. *et al.* A closer look at TCR germline recognition. *Immunity* **36**, 887-888 (2012).

11. Call, M.E., Pyrdol, J., Wiedmann, M. & Wucherpfennig, K.W. The organizing principle in the formation of the T cell receptor-CD3 complex. *Cell* **111**, 967-979 (2002).

12. Dong *et al.* Structural basis of assembly of the human T cell receptor-CD3 complex. *Nature* **573**, 546-552 (2019).

13. He, Y. *et al.* Identification of the Docking Site for CD3 on the T Cell Receptor beta Chain by Solution NMR. *The Journal of biological chemistry* **290**, 19796-19805 (2015).

14. Natarajan, A. *et al.* Structural Model of the Extracellular Assembly of the TCR-CD3 Complex. *Cell Rep* **14**, 2833-2845 (2016).

15. Nika, K. *et al.* Constitutively active Lck kinase in T cells drives antigen receptor signal transduction. *Immunity* **32**, 766-777 (2010).

16. Acuto, O., Di Bartolo, V. & Michel, F. Tailoring T-cell receptor signals by proximal negative feedback mechanisms. *Nature reviews. Immunology* **8**, 699-712 (2008).

17. Huse, M. *et al.* Spatial and temporal dynamics of T cell receptor signaling with a photoactivatable agonist. *Immunity* **27**, 76-88 (2007).

18. DeFord-Watts, L.M. *et al.* The cytoplasmic tail of the T cell receptor CD3 epsilon subunit contains a phospholipid-binding motif that regulates T cell functions. *Journal of immunology* **183**, 1055-1064 (2009).

19. Xu, C. *et al.* Regulation of T cell receptor activation by dynamic membrane binding of the CD3epsilon cytoplasmic tyrosine-based motif. *Cell* **135**, 702-713 (2008).

20. Gil, D., Schamel, W.W., Montoya, M., Sanchez-Madrid, F. & Alarcon, B. Recruitment of Nck by CD3 epsilon reveals a ligand-induced conformational change essential for T cell receptor signaling and synapse formation. *Cell* **109**, 901-912 (2002).

21. Cochran, J.R., Aivazian, D., Cameron, T.O. & Stern, L.J. Receptor clustering and transmembrane signaling in T cells. *Trends Biochem Sci* **26**, 304-310 (2001).

22. Yokosuka, T. *et al.* Newly generated T cell receptor microclusters initiate and sustain T cell activation by recruitment of Zap70 and SLP-76. *Nature immunology* **6**, 1253-1262 (2005).

23. Delon, J. *et al.* CD8 expression allows T cell signaling by monomeric peptide-MHC complexes. *Immunity* **9**, 467-473 (1998).

24. Davis, S.J. & van der Merwe, P.A. The kinetic-segregation model: TCR triggering and beyond. *Nature immunology* **7**, 803-809 (2006).

25. Kim, S.T. *et al.* The alphabeta T cell receptor is an anisotropic mechanosensor. *The Journal of biological chemistry* **284**, 31028-31037 (2009).

26. Liu, B., Chen, W., Evavold, B.D. & Zhu, C. Accumulation of dynamic catch bonds between TCR and agonist peptide-MHC triggers T cell signaling. *Cell* **157**, 357-368 (2014).

27. Minguet, S., Swamy, M., Alarcon, B., Luescher, I.F. & Schamel, W.W. Full activation of the T cell receptor requires both clustering and conformational changes at CD3. *Immunity* **26**, 43-54 (2007).

28. Kjer-Nielsen, L. *et al.* A structural basis for the selection of dominant alphabeta T cell receptors in antiviral immunity. *Immunity* **18**, 53-64 (2003).

29. Beddoe, T. *et al.* Antigen ligation triggers a conformational change within the constant domain of the alphabeta T cell receptor. *Immunity* **30**, 777-788 (2009).

30. Hawse, W.F. *et al.* Cutting edge: Evidence for a dynamically driven T cell signaling mechanism. *Journal of immunology* **188**, 5819-5823 (2012).

31. Natarajan, K. *et al.* An allosteric site in the T-cell receptor Cbeta domain plays a critical signalling role. *Nature communications* **8**, 15260 (2017).

32. Rangarajan, S. *et al.* Peptide-MHC (pMHC) binding to a human antiviral T cell receptor induces long-range allosteric communication between pMHC- and CD3-binding sites. *The Journal of biological chemistry* **293**, 15991-16005 (2018).

33. Chen, J.L. *et al.* Structural and kinetic basis for heightened immunogenicity of T cell vaccines. *The Journal of experimental medicine* **201**, 1243-1255 (2005).

34. Alcover, A., Mariuzza, R.A., Ermonval, M. & Acuto, O. Lysine 271 in the transmembrane domain of the T-cell antigen receptor beta chain is necessary for its assembly with the CD3 complex but not for alpha/beta dimerization. *The Journal of biological chemistry* **265**, 4131-4135 (1990).

35. McKeithan, T.W. Kinetic proofreading in T-cell receptor signal transduction. *Proc Natl Acad Sci U S A* **92**, 5042-5046 (1995).

36. Dushek, O. *et al.* Antigen potency and maximal efficacy reveal a mechanism of efficient T cell activation. *Sci Signal* **4**, ra39 (2011).

37. Stachlewitz, R.F. *et al.* A-770041, a novel and selective small-molecule inhibitor of Lck, prevents heart allograft rejection. *J Pharmacol Exp Ther* **315**, 36-41 (2005).

38. Feige, M.J. & Hendershot, L.M. Quality control of integral membrane proteins by assembly-dependent membrane integration. *Mol Cell* **51**, 297-309 (2013).

39. Testi, R., Alcover, A., Spagnoli, G., Reinherz, E.L. & Acuto, O. CD3Ti+ human thymocyte-derived clones displaying a differential response to activation via CD3Ti and CD2. *Cell Immunol* **122**, 350-364 (1989).

40. Swamy, M., Dopfer, E.P., Molnar, E., Alarcon, B. & Schamel, W.W. The 450 kDa TCR Complex has a Stoichiometry of alphabetagammaepsilondeltaepsilonzetazeta. *Scand J Immunol* **67**, 418-420; author reply 421 (2008).

41. Alcover, A., Alarcon, B. & Di Bartolo, V. Cell Biology of T Cell Receptor Expression and Regulation. *Annual review of immunology* **36**, 103-125 (2018).

42. Gupta, K. *et al.* The role of interfacial lipids in stabilizing membrane protein oligomers. *Nature* **541**, 421-424 (2017).

43. Circosta, P. *et al.* T cell receptor (TCR) gene transfer with lentiviral vectors allows efficient redirection of tumor specificity in naive and memory T cells without prior stimulation of endogenous TCR. *Hum Gene Ther* **20**, 1576-1588 (2009).

44. Changeux, J.P. & Christopoulos, A. Allosteric Modulation as a Unifying Mechanism for Receptor Function and Regulation. *Cell* **166**, 1084-1102 (2016).

45. Volkman, B.F., Lipson, D., Wemmer, D.E. & Kern, D. Two-state allosteric behavior in a single-domain signaling protein. *Science* **291**, 2429-2433 (2001).

46. Abd Halim, K.B., Koldso, H. & Sansom, M.S. Interactions of the EGFR juxtamembrane domain with PIP2-containing lipid bilayers: Insights from multiscale molecular dynamics simulations. *Biochim Biophys Acta* **1850**, 1017-1025 (2015).

47. Irving, M. *et al.* Interplay between T cell receptor binding kinetics and the level of cognate peptide presented by major histocompatibility complexes governs CD8+ T cell responsiveness. *The Journal of biological chemistry* **287**, 23068-23078 (2012).

48. Cole, D.K. *et al.* Human TCR-binding affinity is governed by MHC class restriction. *J Immunol* **178**, 5727-5734 (2007).

49. Varela-Rohena, A. *et al.* Control of HIV-1 immune escape by CD8 T cells expressing enhanced T-cell receptor. *Nat Med* **14**, 1390-1395 (2008).

50. Paster, W. *et al.* A THEMIS:SHP1 complex promotes T-cell survival. *The EMBO journal* **34**, 393-409 (2015).

51. Irvine, D.J., Purbhoo, M.A., Krogsgaard, M. & Davis, M.M. Direct observation of ligand recognition by T cells. *Nature* **419**, 845-849 (2002).

52. Lewis, R.S. Store-Operated Calcium Channels: From Function to Structure and Back Again. *Cold Spring Harb Perspect Biol* (2019).

53. Huppa, J.B. *et al.* TCR-peptide-MHC interactions in situ show accelerated kinetics and increased affinity. *Nature* **463**, 963-967 (2010).

54. O'Donoghue, G.P., Pielak, R.M., Smoligovets, A.A., Lin, J.J. & Groves, J.T. Direct single molecule measurement of TCR triggering by agonist pMHC in living primary T cells. *Elife* **2**, e00778 (2013).

55. Mariuzza, R.A., Agnihotri, P. & Orban, J. The structural basis of T-cell receptor (TCR) activation: An enduring enigma. *The Journal of biological chemistry* **295**, 914-925 (2020).

56. Wang, F., Beck-Garcia, K., Zorzin, C., Schamel, W.W. & Davis, M.M. Inhibition of T cell receptor signaling by cholesterol sulfate, a naturally occurring derivative of membrane cholesterol. *Nature immunology* **17**, 844-850 (2016).

57. He, Y. *et al.* Peptide-MHC Binding Reveals Conserved Allosteric Sites in MHC Class I- and Class II-Restricted T Cell Receptors (TCRs). *J Mol Biol* (2020).

58. Wang, Y. *et al.* A conserved CXXC motif in CD3epsilon is critical for T cell development and TCR signaling. *PLoS Biol* **7**, e1000253 (2009).

59. Chouaki-Benmansour, N. *et al.* Phosphoinositides regulate the TCR/CD3 complex membrane dynamics and activation. *Scientific reports* **8**, 4966 (2018).

60. Swamy, M. *et al.* A Cholesterol-Based Allostery Model of T Cell Receptor Phosphorylation. *Immunity* **44**, 1091-1101 (2016).

61. Das, D.K. *et al.* Force-dependent transition in the T-cell receptor beta-subunit allosterically regulates peptide discrimination and pMHC bond lifetime. *Proc Natl Acad Sci U S A* **112**, 1517-1522 (2015).

62. Beemiller, P. & Krummel, M.F. Mediation of T-cell activation by actin meshworks. *Cold Spring Harb Perspect Biol* **2**, a002444 (2010).

63. Boniface, J.J. *et al.* Initiation of signal transduction through the T cell receptor requires the multivalent engagement of peptide/MHC ligands [corrected]. *Immunity* **9**, 459-466 (1998).

64. Varma, R., Campi, G., Yokosuka, T., Saito, T. & Dustin, M.L. T cell receptor-proximal signals are sustained in peripheral microclusters and terminated in the central supramolecular activation cluster. *Immunity* **25**, 117-127 (2006).

65. Zhu, C., Chen, W., Lou, J., Rittase, W. & Li, K. Mechanosensing through immunoreceptors. *Nature immunology* **20**, 1269-1278 (2019).

66. Hong, J. *et al.* A TCR mechanotransduction signaling loop induces negative selection in the thymus. *Nature immunology* **19**, 1379-1390 (2018).

67. Kern, D. & Zuiderweg, E.R. The role of dynamics in allosteric regulation. *Curr Opin Struct Biol* **13**, 748-757 (2003).

68. Tzeng, S.R. & Kalodimos, C.G. Protein activity regulation by conformational entropy. *Nature* **488**, 236-240 (2012).

69. Jiang, N. *et al.* Two-stage cooperative T cell receptor-peptide major histocompatibility complex-CD8 trimolecular interactions amplify antigen discrimination. *Immunity* **34**, 13-23 (2011).

70. Casas, J. *et al.* Ligand-engaged TCR is triggered by Lck not associated with CD8 coreceptor. *Nature communications* **5**, 5624 (2014).

71. Brameshuber, M. *et al.* Monomeric TCRs drive T cell antigen recognition. *Nature immunology* **19**, 487-496 (2018).

72. Freed, D.M. *et al.* EGFR Ligands Differentially Stabilize Receptor Dimers to Specify Signaling Kinetics. *Cell* **171**, 683-695 e618 (2017).

73. Furness, S.G.B. *et al.* Ligand-Dependent Modulation of G Protein Conformation Alters Drug Efficacy. *Cell* **167**, 739-749 e711 (2016).

74. Lane, J.R., May, L.T., Parton, R.G., Sexton, P.M. & Christopoulos, A. A kinetic view of GPCR allostery and biased agonism. *Nat Chem Biol* **13**, 929-937 (2017).

Acknowledgements

Financial support: Wellcome Trust WT200844/Z/16/Z to O.A.; WT092970MA and WT208361/Z/17/Z to M.S.P.S.; WT100262Z/12/Z to M.L.D.; 207537/Z/17/Z to O.D.; SBF002\1031 to A.C.K. Springboard Award and WT. ERC-2014-AdG 670930 to S.B. Care-for-Rare Postgraduate Fellowship to A-L.L. For MDS, High-Performance Computing facilities, University of Leeds. We thank Juliane Cohen, Christine Ralf and Salvatore Valvo for technical support and John Orban, Brian Baker, Ian Wilson, Pedro Carvalho, Marco Fritzsche, Hai-Tao He, Immanuel Luescher, Cheng Zhu, Andrew Sewell for discussions, suggestions and for reading the manuscript; C.R. and J.C. for manuscript editing.

Author contributions

Conceptualization, O.A.
Methodology, A-L.L.; G.M.; N.P.; A.C.; D.C.; R.R.; D.K.C.; M.L.; S.B.; A.C.K.; D.P.; O.D.; M.L.D.; M.S.P.S.; O.A.
Software, A.C.K.; O.D.
Formal Data Analysis, A-L.L.; G.M.; N.P.; A.C.; D.C.; D.P.; S.B.; O.D.; M.S.P.S.; O.A.
Investigation, A-L.L.; G.M.; N.P.; A.C.; D.C.; A.C.K.; S.B.; D.G.; D.K.C.; D.P.; M.S.P.S.; O.A.
Resources, S.B.
Writing - Original Draft, O.A.
Writing - Review and Editing, O.A.; A-L.L.; G.M.; N.P.; A.C.; D.P.; A.C.K.; M.S.P.S.; D.K.C.; M.L.; M.L.D. and D.C.
Visualization, G.M.; A-L.L.; N.P.; A.C.K.; A.C.; D.C.; D.P.; D.K.C.; S.B.; O.A.
Supervision, A.C.K.; M.S.P.S.; M.L.D.; O.A.
Funding acquisition, A.C.K.; M.S.P.S.; M.L.D.; O.A.

Declaration of Interests

"The authors declare no competing interests”

Materials and Correspondence

Correspondence and requests for materials should be addressed to O.A.

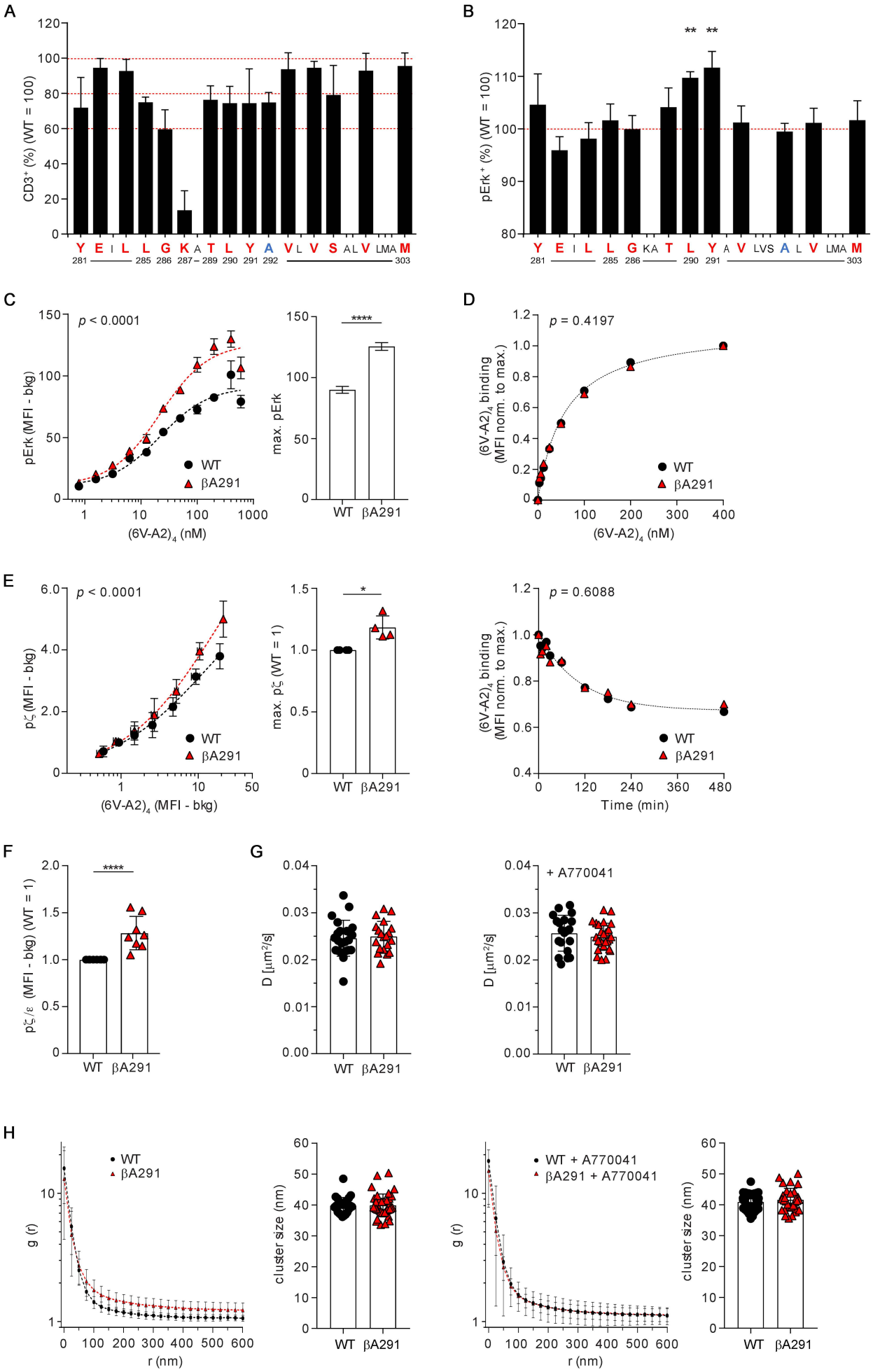
A
CD3+ (%) (WT = 100)
Y E I L L G K A T L Y A V L V S A L V LMA M
281 285 286 287 289 290 291 292 303
B
pErk+ (%) (WT = 100)
** **
Y E I L L G KA T L Y A V LVS A L V LMA M
281 285 286 290 291 303
C
p < 0.0001
pErk (MFI - bkg)
(6V-A2)4 (nM)
WT
βA291
****
max. pErk
D
p = 0.4197
(6V-A2)4 binding (MFI norm. to max.)
(6V-A2)4 (nM)
E
p < 0.0001
pζ (MFI - bkg)
(6V-A2)4 (MFI - bkg)
*
max. pζ (WT = 1)
p = 0.6088
Time (min)
F
****
pζ/ε (MFI - bkg) (WT = 1)
G
D [μm2/s]
+ A770041
H
g (r)
r (nm)
cluster size (nm)
WT + A770041
βA291 + A770041

Fig 1

Figure 1. Gain-of-function mutations in β TMR

A CD3 surface expression of 1G4-WT and mutants. x̄±SD of $CD3^+$ cells, n=3-8. Ala (red), Leu (blue) substitution. **B** pErk response of 1G4-WT and β mutants stimulated with $(6V\text{-}A2)_4$. x̄±SEM of $pErk^+$ cells, n=3-6, unpaired *t*-test *p*=0.0011 (βA290), *p*=0.0092 (βA291). **C** pErk response of CD8-deficient J76 1G4-WT and 1G4-βA291 stimulated with the indicated concentrations of $(6V\text{-}A2)_4$. **Left**, non-linear regression fit of $(6V\text{-}A2)_4$ nM vs. pErk MFI, n=3, R^2=0.82 (WT), 0.89 (βA291); EC_{50}=19.5±5.5 (WT), 19.0±3.1 (βA291). **Right**, x̄±SD of max. pErk, n=3, F-test *p*<0.0001. See also Fig. **S1E**. **D** $(6V\text{-}A2)_4$ binding to 1G4-WT or 1G4-βA291. **Top**, $(6V\text{-}A2)_4$ dose-dependent association, n=3, non-linear regression fit, R^2=0.98 (WT), 0.97 (βA291), F-test (ns). **Bottom**, $(6V\text{-}A2)_4$ dissociation rate, n=5, non-linear regression fit, R^2=0.84 (WT), 0.72 (βA291), F-test (ns). **E** pζ response of J76 1G4-WT or 1G4-βA291 stimulated with $(6V\text{-}A2)_4$. **Left**, non-linear regression fit of $(6V\text{-}A2)_4$ MFI vs. pζ MFI, n=3, R^2=0.95 (WT), 0.96 (βA291). **Right**, x̄±SD of max. pζ, n=4, unpaired *t*-test *p*=0.0078. See also Fig. **S1F**. **F** Basal pζ in J76 1G4-WT or 1G4-βA291. pζ MFI normalised to surface CD3 MFI, n=8, unpaired *t*-test *p*<0.0001. See also Figs. **S1H** and **S1I**. **G** FRAP of 1G4-WT or 1G4-βA291, treated (**right**) or not (**left**) with A770041. x̄±SD of diffusion coefficient, D ($\mu m^2/s$), n≥20 cells, *t*-test (ns). **H** Lateral distribution by dSTORM of 1G4-WT or 1G4-βA291, treated (**right**) or not (**left**) with A770041. Plots represent pair auto-correlation analysis (g), x̄±SD of ≥25 cells. Histograms show DBSCAN cluster analysis, x̄±SD of cluster size per cell, *t*-test (ns).

A

anti-HA (β) PD

WT WT βA291

\+ - - HA peptide

IB:

50 - β (β_1, β_2, β_3)

20 - ε

15 - ζ

****

ε/β_T (WT = 1)

ζ/β_2 (WT = 1)

WT βA291

Input lysates

WT βA291

IB:

50 - β

20 - ε

15 - ζ

37 - actin

β_T/actin (WT = 1)

ε/actin (WT = 1)

ζ/actin (WT = 1)

B

anti-HA (β) PD

WT WT βA291

\+ - - HA peptide

IB:

100 - β

25 - γ

(NR)

γ/β_T (WT = 1)

C

anti-HA (β) PD

WT βA291 WT

\- - + HA peptide

IB:

100 - β

20 - δ

(NR)

δ/β_T (WT = 1)

D

Extracellular view

CD3δ

TCRβ

CD3ε

TCRα

CD3ε

CD3γ

ζ_2

ζ_1

90°

Transmembrane view of βY291 interactions

Y291

L129

L145

N263

T267

G132

Fig 2

Figure 2. βY291 contribution to TCR-CD3 quaternary structure cohesion

A Anti-HA (β-HA) Pull Down (PD) and IB of 1G4-WT or 1G4-βA291. **Upper panels: left**, IB: 1 of 5 experiments, arrows indicate β-isoforms; **right**, x̄±SD of ε/β_T and ζ/β_2, n=5, unpaired *t*-test $p<0.0001$. **Bottom panels:** input lysates, **left**, IB: 1 of 5 experiments; **right**, x̄±SD of β_T/actin, ε/actin and ζ/actin, n=5, unpaired *t*-test (ns). **B** β-HA PD and IB of 1G4-WT or 1G4-βA291. (NR) non-reducing conditions. **Left**, IB: 1 of 4 experiments. **Right**, x̄±SD of γ/β_T, n=4, unpaired *t*-test $p<0.0001$. **C** β-HA PD and IB of 1G4-WT or 1G4-βA291. (NR) non-reducing conditions. **Left**, IB: 1 of 4 experiments. **Right**, x̄±SD of δ/β_T, n=4, unpaired *t*-test $p<0.0001$. **D** All-atom MDS of TCR-CD3 TMRs. TCRα (ochre), TCRβ (grey), CD3δ (blue), CD3ε (yellow), CD3γ (green), ζ (red). **Left**, extracellular view of a snapshot of TCR-CD3 TMRs. **Right**, βY291 interactions with TCR-CD3 TMRs. Significant contacts of βY291 with TCRα, CD3γ and CD3ε are shown as liquorice sticks. See also Fig. **S2G**.

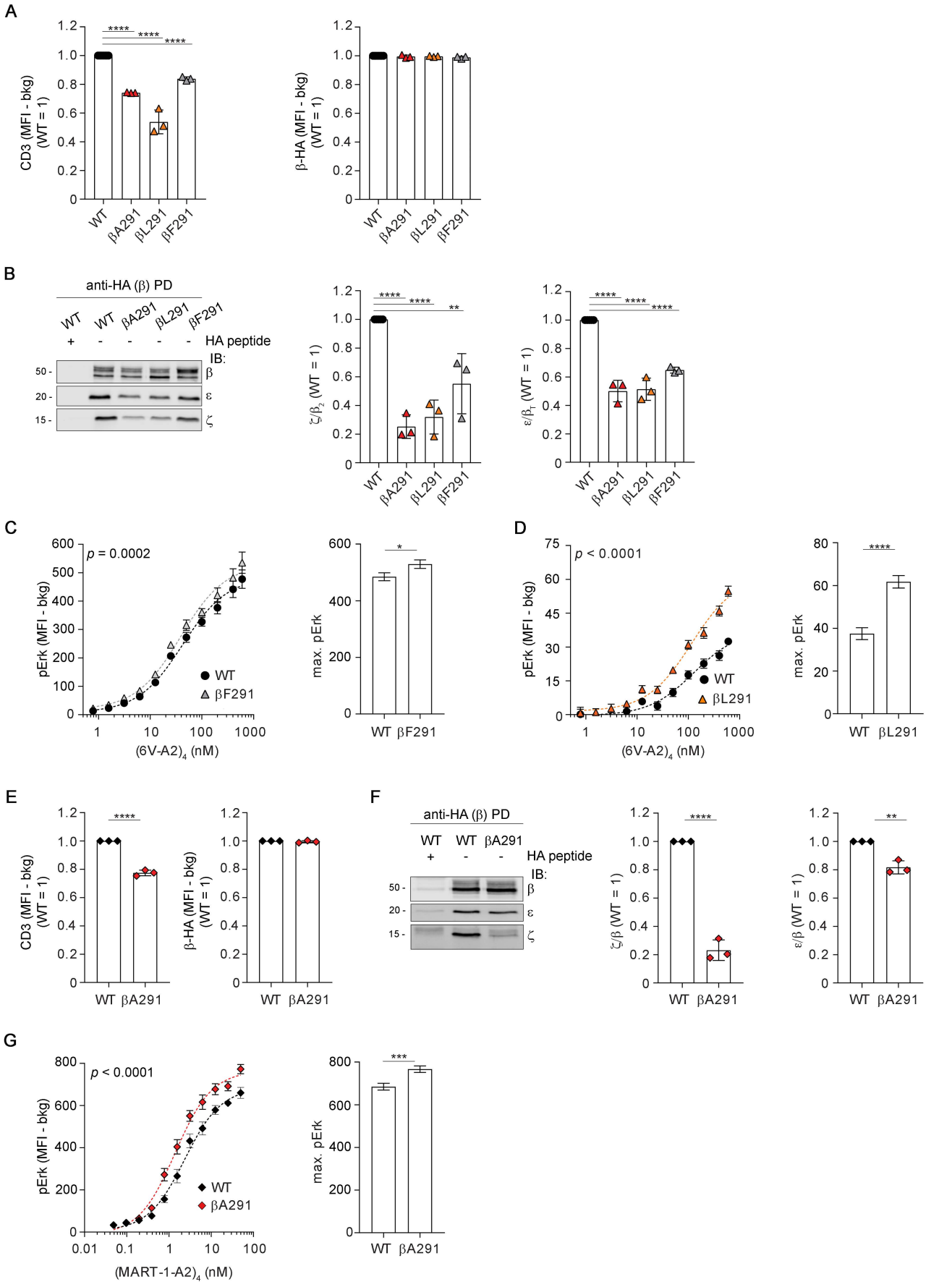
A
CD3 (MFI - bkg) (WT = 1)
β-HA (MFI - bkg) (WT = 1)
WT
βA291
βL291
βF291
B
anti-HA (β) PD
HA peptide
IB:
ζ/β2 (WT = 1)
ε/β1 (WT = 1)
C
p = 0.0002
pErk (MFI - bkg)
(6V-A2)4 (nM)
max. pErk
D
p < 0.0001
E
F
G
p < 0.0001
(MART-1-A2)4 (nM)

Fig 3

Figure 3. Loosening ζ association enhances signalling

A TCR-CD3 expression of 1G4-WT, 1G4-βA291, 1G4-βL291, 1G4-βF291 in CD8-deficient J76. **Left**, x̄±SEM of CD3 MFI in HA^{low}gate, n=3, unpaired *t*-test $p<0.0001$. **Right**, x̄±SEM of β-HA MFI in HA^{low}gate, n=3, *t*-test (ns). **B** β-HA PD and IB of 1G4-WT or the indicated 1G4-β mutants. **Left**, IB: 1 of 3 experiments. **Middle**, x̄±SD of ζ/β_2, n=3, unpaired *t*-test WT vs. βA291, WT vs. βL291 $p<0.0001$, WT vs. βF291 $p<0.01$. **Right**, x̄±SD of ε/β_T, n=3, unpaired *t*-test $p<0.0001$. **C** pErk response of CD8-deficient J76 1G4-WT or 1G4-βF291 stimulated with the indicated concentrations of $(6V\text{-}A2)_4$. **Left**, non-linear regression fit of $(6V\text{-}A2)_4$ nM vs. pErk MFI, n=3, R^2=0.915 (WT), 0.910 (βF291). **Right**, x̄±SD of max. pErk, n=3, F-test $p<0.05$. See also Fig. **S3A** (**left**). **D** pErk response of CD8-deficient J76 1G4-WT or 1G4-βL291 stimulated with the indicated concentrations of $(6V\text{-}A2)_4$. **Left**, non-linear regression fit of $(6V\text{-}A2)_4$ nM vs. pErk MFI, n=3, R^2=0.827 (WT), 0.910 (βL291). **Right**, x̄±SD of max. pErk, n=3, F-test $p<0.0001$. See also Fig. **S3A** (**right**). **E** TCR-CD3 expression in CD8-deficient J76 2H5-WT or 2H5-βA291. **Left**, x̄±SEM of CD3 MFI in HA^{low}gate, n=3, unpaired *t*-test $p<0.0001$. **Right**, x̄±SEM of β-HA MFI in HA^{low}gate, n=3, *t*-test (ns). **F** β-HA PD and IB of 2H5-WT or 2H5-βA291. **Left**, IB: 1 of 3 experiments. **Middle**, x̄±SD of ζ/β, n=3, unpaired *t*-test $p<0.0001$. **Right**, x̄±SD of ε/β, n=3, unpaired *t*-test $p<0.01$. **G** pErk response of CD8-deficient J76 2H5-WT or 2H5-βA291 stimulated with the indicated concentrations of $(MART\text{-}1\text{-}A2)_4$. **Left**, non-linear regression fit of $(MART\text{-}1\text{-}A2)_4$ nM vs. pErk MFI, n=3, R^2=0.94 (WT), 0.94 (βA291). **Right**, x̄±SD of max. pErk, n=3, F-test $p<0.001$. See also Fig. **S3G**.

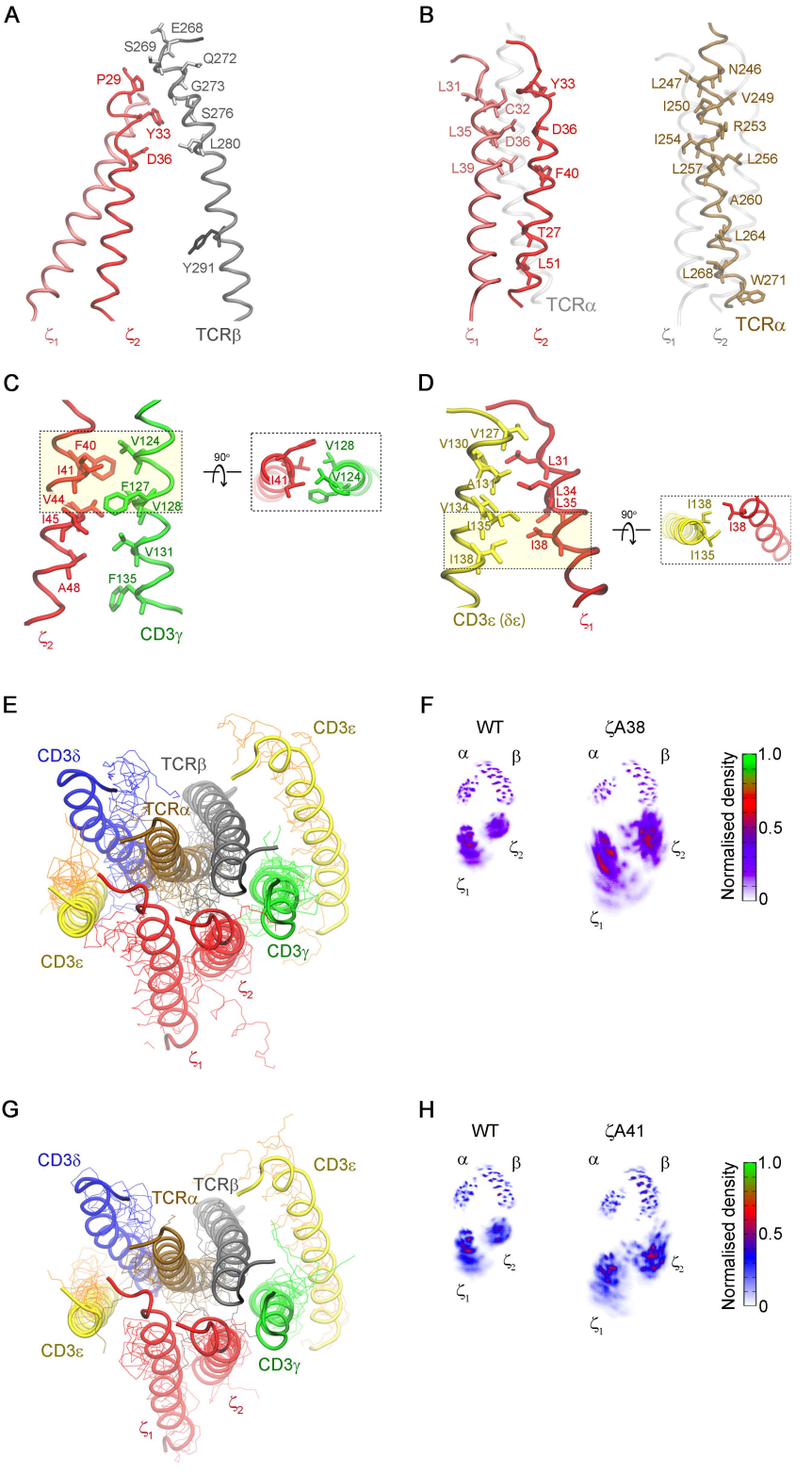
A
E268
S269
Q272
P29
G273
S276
Y33
L280
D36
Y291
ζ1
ζ2
TCRβ
B
L31
Y33
C32
L35
D36
D36
L39
F40
T27
L51
TCRα
ζ1
ζ2
N246
L247
V249
I250
R253
I254
L256
L257
A260
L264
L268
W271
TCRα
ζ1
ζ2
C
F40
V124
I41
F127
V44
V128
I45
V131
F135
A48
ζ2
CD3γ
90°
V128
I41
V124
D
V130
V127
L31
A131
L34
L35
V134
I135
I38
I138
CD3ε (δε)
ζ1
90°
I138
I38
I135
E
CD3δ
TCRβ
CD3ε
TCRα
CD3ε
CD3γ
ζ2
ζ1
F
WT
ζA38
α
β
α
β
ζ2
ζ1
ζ2
ζ1
Normalised density
1.0
0.5
0
G
CD3δ
TCRβ
CD3ε
TCRα
CD3ε
CD3γ
ζ2
ζ1
H
WT
ζA41
α
β
α
β
ζ2
ζ1
ζ2
ζ1
Normalised density
1.0
0.5
0

Fig 4

Figure 4. Loosening ζ association enhances signalling

A Snapshot from all-atom MDS of TCR-CD3 TMRs. Contacts between TCRβ (grey), ζ_1 (light red) and ζ_2 (dark red) TMRs. See also Fig. **S4A**. βY291 is represented as liquorice stick for reference and does not contact ζζ. **B** Snapshot from all-atom MDS of TCR-CD3 TMRs. **Left**, ζ_1 (light red) and ζ_2 (dark red) residues contacting TCRα TMR (in transparency). **Right**, TCRα (ochre) residues contacting ζ_1 and ζ_2 TMRs (in transparency). See also Fig. **S4B**. **C** Snapshot from all-atom MDS of TCR-CD3 TMRs. **Left**, contacts between ζ_2 (red) and CD3γ (green) TMRs. **Right**, Top view of ζ_2I41 (red) contacts with CD3γ (green). See also Figs. **S4C** and **S4F**. **D** Snapshot from all-atom MDS of TCR-CD3 TMRs. **Left**, contacts between ζ_1 (red) and CD3ε (δε) (yellow) TMRs. **Right**, Top view of ζ_1I38 (red) contacts with CD3ε (δε) (yellow). See also Figs. **S4D** and **S4E**. **E** Snapshot from all-atom MDS of TCR-CD3 TMRs carrying ζA38 (lines) aligned to ζWT (cartoon) at the end of 1250ns MDS. TCRα (ochre), TCRβ (grey), CD3δ (blue), CD3ε (yellow), CD3γ (green), ζ (red). See also Figs. **S4G**-**S4J**. **F** Normalised spatial distributions of the Cα atoms of ζζ relative to the Cα atoms of TCRαβ in ζWT and ζA38. **G** Snapshot from all-atom MDS of TCR-CD3 TMRs carrying ζA41 (lines) aligned to ζWT (cartoon) at the end of 1250ns MDS. TCRα (ochre), TCRβ (grey), CD3δ (blue), CD3ε (yellow), CD3γ (green), ζ (red). See also Figs. **S4K**-**S4N**. **H** Normalised spatial distributions of the Cα atoms of ζζ relative to the Cα atoms of TCRαβ in ζWT and ζA41.

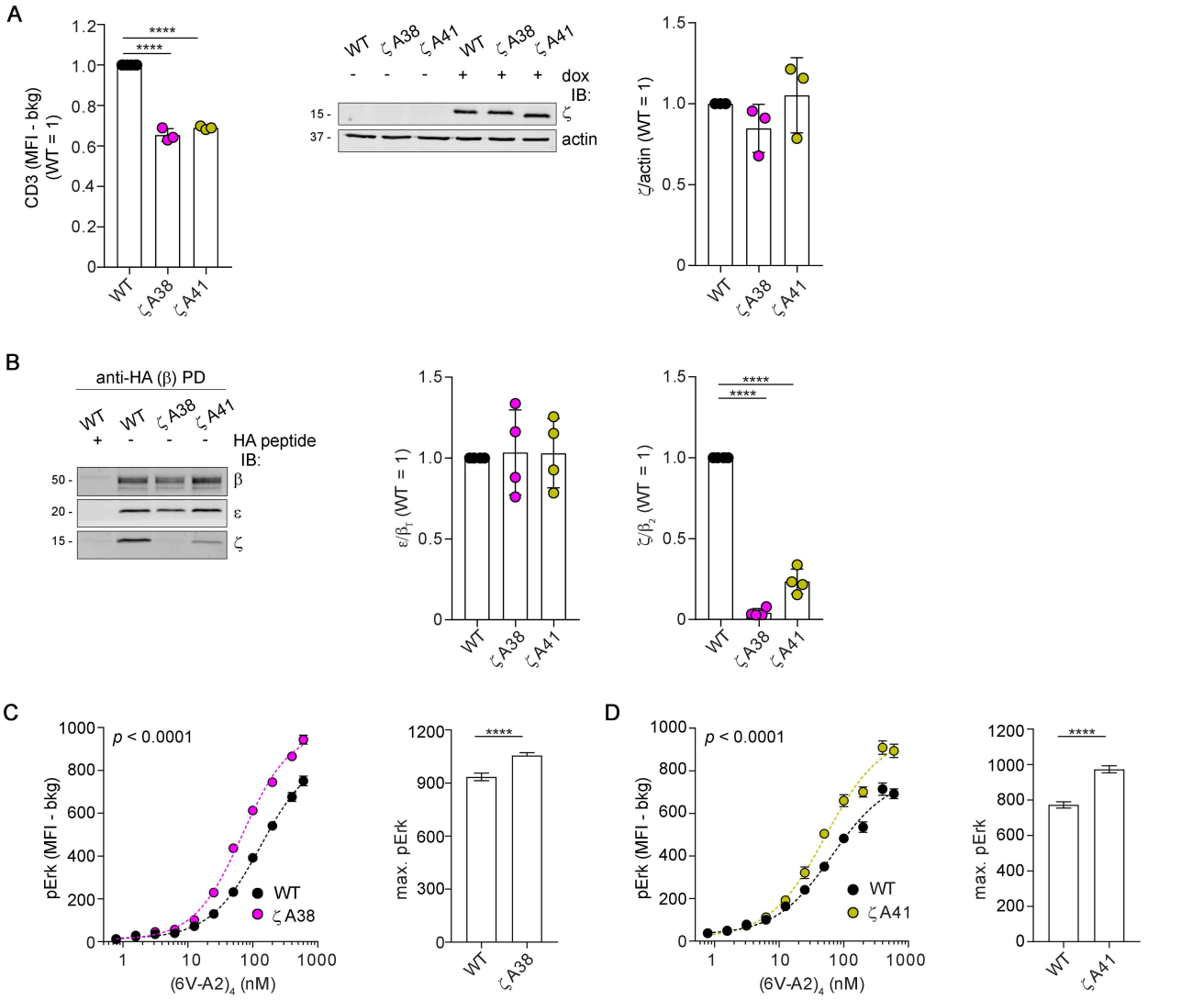
A
CD3 (MFI - bkg) (WT = 1)
****
****
WT
ζA38
ζA41
dox
IB:
15 -
37 -
ζ
actin
ζ/actin (WT = 1)
B
anti-HA (β) PD
HA peptide
IB:
50 -
20 -
15 -
β
ε
ζ
ε/β1 (WT = 1)
ζ/β2 (WT = 1)
C
p < 0.0001
pErk (MFI - bkg)
(6V-A2)4 (nM)
max. pErk
D
p < 0.0001

Fig 5

Figure 5. Loosening ζ association enhances signalling

A TCR-CD3 expression in J76-1G4WT-ζKO expressing ζWT or ζA38 or ζA41. **Left**, x̄±SEM of CD3 MFI in HA^{low} gate, n=3, unpaired *t*-test $p<0.0001$. **Middle**, IB: 1 of 3 experiments. **Right**, x̄±SD of ζ/actin, n=3, unpaired *t*-test (ns). **B** β-HA PD and IB of 1G4-WT carrying ζWT or ζA38 or ζA41. **Left**, IB: 1 of 4 PD. **Right**, x̄±SD of ε/β_T and ζ/β_2, n=4, unpaired *t*-test $p<0.0001$. **C** J76-1G4WT-ζKO expressing ζWT or ζA38 stimulated with the indicated concentrations of $(6V\text{-}A2)_4$. **Left**, non-linear regression fit of $(6V\text{-}A2)_4$ nM vs. pErk MFI, n=3, R^2=0.98 (WT), 0.99 (ζA38). **Right**, x̄±SD of max. pErk, n=3, F-test $p<0.0001$. See also Fig. **S5B**. **D** pErk response of J76-1G4WT-ζKO expressing ζWT or ζA41 stimulated with $(6V\text{-}A2)_4$. **Left**, non-linear regression fit of $(6V\text{-}A2)_4$ nM vs. pErk MFI, n=3, R^2=0.96 (WT), 0.97 (ζA41). **Right**, x̄±SD of max. pErk, n=3, F-test $p<0.0001$. See also Fig. **S5C**.

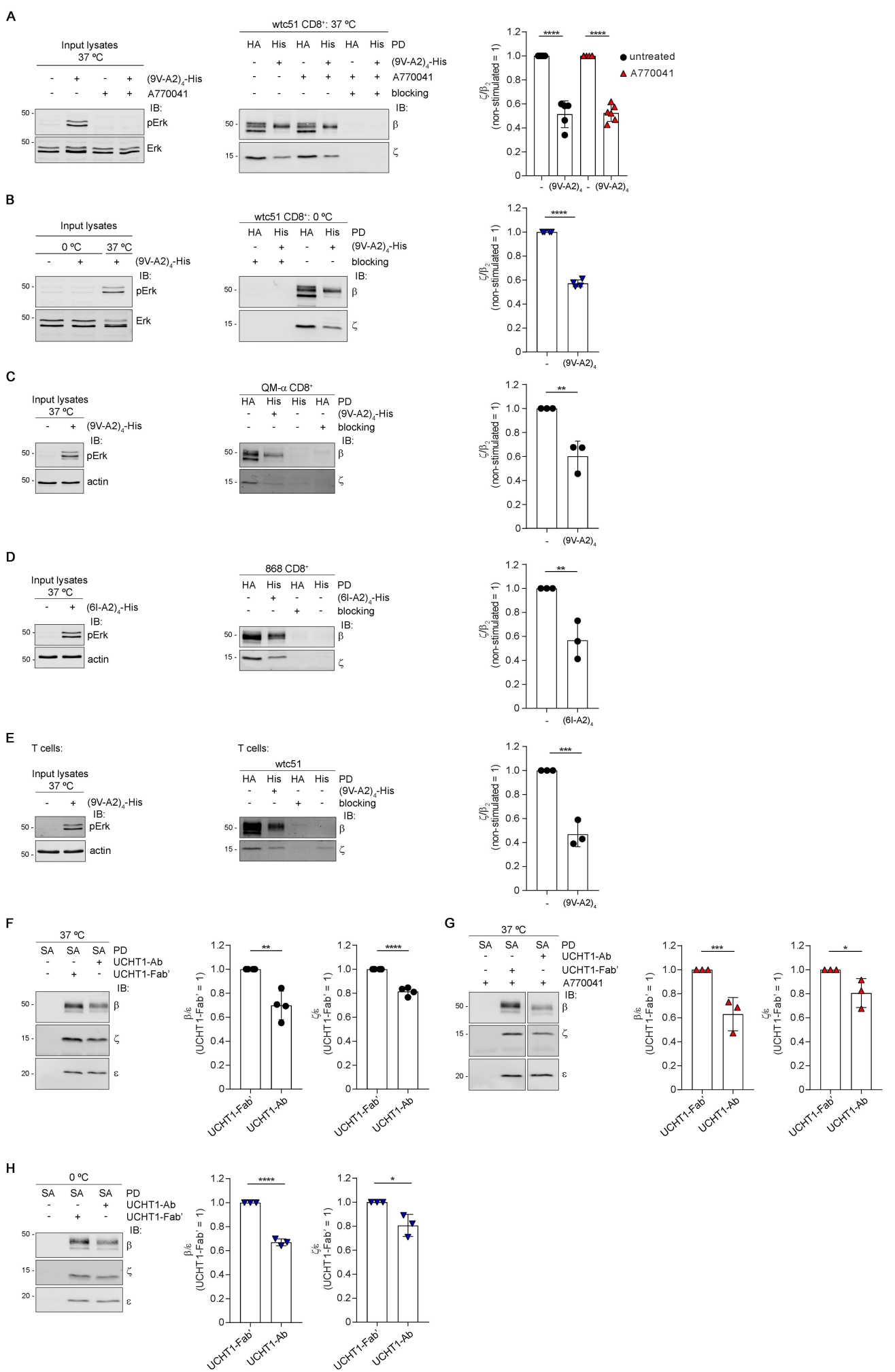
A
Input lysates
37 ºC
(9V-A2)4-His
A770041
IB:
pErk
Erk
wtc51 CD8+: 37 ºC
HA His HA His HA His PD
(9V-A2)4-His
A770041
blocking
β
ζ
untreated
A770041
ζ/β2 (non-stimulated = 1)
B
Input lysates
0 ºC 37 ºC
wtc51 CD8+: 0 ºC
C
QM-α CD8+
actin
D
868 CD8+
(6I-A2)4-His
E
T cells:
wtc51
F
37 ºC
SA SA SA PD
UCHT1-Ab
UCHT1-Fab'
ε
β/ε (UCHT1-Fab' = 1)
ζ/ε (UCHT1-Fab' = 1)
G
H
0 ºC

Fig 6

Figure 6. pMHC tetramer binding loosens αβ association with ζ

A J76 wtc51 stimulated with $(9V\text{-}A2)_4$-His ±A770041. **Left**, pErk response (1 of 4 experiments). **Middle**, PD with anti-HA Ab (HA) (lanes 1, 3, 5) or His-Cobalt beads (His) (lanes 2, 4, 6) followed by IB for β and ζ. Blocking was with HA peptide or imidazole. 1 of 6 experiments. **Right**, x̄±SD of ζ/β_2, n=5-6, unpaired *t*-test $p<0.0001$. **B** J76 wtc51 stimulated with $(9V\text{-}A2)_4$-His at 0°C. **Left**, pErk response (1 of 4 experiments). **Middle**, β-HA (lanes 1, 3) or His (lanes 2, 4) PD and IB for β and ζ (1 experiment of 4). **Right**, x̄±SD of ζ/β_2, n=4, unpaired *t*-test $p<0.0001$. **C** J76 QM-α stimulated with $(9V\text{-}A2)_4$-His. **Left**, pErk response (1 of 3 experiments). **Middle**, β-HA (lanes 1, 4) or His (lanes 2, 3) PD and IB for β and ζ (1 experiment of 3). **Right**, x̄±SD of ζ/β_2, n=3, unpaired *t*-test $p<0.01$. **D** J76 868 stimulated with $(6I\text{-}A2)_4$-His. **Left**, pErk response (1 of 3 experiments). **Middle**, β-HA (lanes 1, 3) or His (lanes 2, 4) PD and IB for β and ζ (1 experiment of 3). **Right**, x̄±SD of ζ/β_2, n=3, unpaired *t*-test $p<0.01$. **E** Primary T cells expressing wtc51 stimulated with $(9V\text{-}A2)_4$-His. **Left**, pErk response (1 of 3 experiments). **Middle**, β-HA (lanes 1, 3) or His (lanes 2, 4) PD and IB for β and ζ (1 experiment of 3). **Right**, x̄±SD of ζ/β_2, n=3, unpaired *t*-test $p<0.001$. **F** J76 1G4 ±UCHT1-Fab' or UCHT1-Ab. **Left**, streptavidin (SA)-mediated PD and IB for β, ζ and ε (1 of 4 experiments). **Right**, x̄±SD of β/ε and ζ/ε, n=4, unpaired *t*-test $p=0.0023$, $p<0.0001$. **G** J76 1G4 ±A770041 incubated or not with UCHT1-Fab' or UCHT1-Ab. **Left**, SA-mediated PD and IB for β, ζ and ε (1 of 3 experiments). See also Fig. **S6D**. **Right**, x̄±SD of β/ε and ζ/ε, n=3, unpaired *t*-test $p=0.0007$, $p=0.0494$. **H** J76 1G4 ±UCHT1-Fab' or UCHT1-Ab at 0°C. **Left**, SA-mediated PD and IB for β, ζ and ε (1 of 3 experiments). **Right**, x̄±SD of β/ε and ζ/ε, n=3, unpaired *t*-test $p<0.0001$, $p=0.0218$. See also Fig. **S6E**.

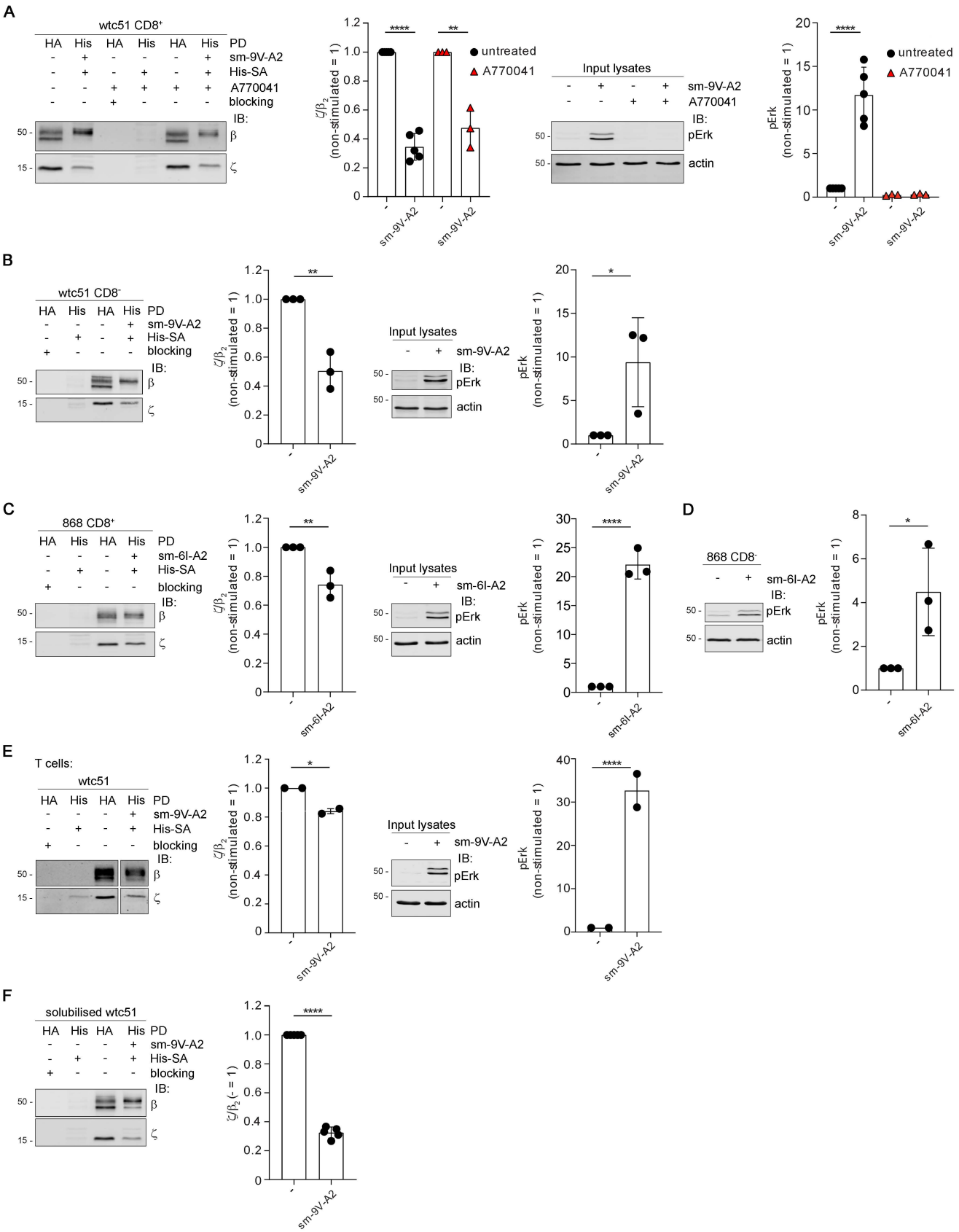
A
wtc51 CD8+
HA His HA His HA His PD
sm-9V-A2
His-SA
A770041
blocking
IB:
β
ζ
ζ/β2 (non-stimulated = 1)
untreated
A770041
Input lysates
sm-9V-A2
A770041
pErk
actin
pErk (non-stimulated = 1)
B
wtc51 CD8-
HA His HA His PD
sm-9V-A2
His-SA
blocking
C
868 CD8+
sm-6I-A2
D
868 CD8-
E
T cells:
wtc51
F
solubilised wtc51
ζ/β2 (- = 1)

Fig 7

Figure 7. Monovalent pMHC in solution triggers TCR-CD3 untying and intracellular signalling

A J76 wtc51 ±A770041 stimulated or not with sm-9V-A2 were lysed and subjected to PD with anti-HA Ab or Talon beads. **First panel**, anti-HA (β-HA) (lanes 1, 3, 5) or Talon beads (His) (lanes 2, 4, 6) PD and IB for β and ζ (1 experiment of 3). **Second panel**, x̄±SD of ζ/β_2, n≥3, unpaired *t*-test $p<0.0001$ and $p<0.01$. **Third panel**, pErk IB: 1 of 3 experiments. **Fourth panel**, x̄±SD of pErk, n≥3, unpaired *t*-test $p<0.0001$. **B** CD8-deficient J76 wtc51 stimulated or not with sm-9V-A2 were processes as in **A**. **First panel**, β-HA (lanes 1, 3) or His (lanes 2, 4) PD and IB for β and ζ (1 of 3 experiments). **Second panel**, x̄±SD of ζ/β_2, n=3, unpaired *t*-test $p<0.01$. **Third panel**, pErk IB (1 of 3 experiments). **Fourth panel**, x̄±SD of pErk, n=3, unpaired *t*-test $p<0.05$. **C** J76 868 stimulated or not with sm-6I-A2 were processes as in **A**. **First panel**, β-HA (lanes 1, 3) or His (lanes 2, 4) PD and IB for β and ζ (1 of 3 experiments). **Second panel**, x̄±SD of ζ/β_2, n=3, unpaired *t*-test $p<0.01$. **Third panel**, pErk IB: 1 of 3 experiments. **Fourth panel**, x̄±SD of pErk, n=3, unpaired *t*-test $p<0.0001$. **D** CD8-deficient J76 868 stimulated or not with sm-6I-A2. **Left**, pErk IB (1 of 3 experiments). Right, x̄±SD of pErk, n=3, unpaired *t*-test $p<0.05$. **E** Primary T cells expressing wtc51 stimulated or not with sm-9V-A2 were processes as in **A**. **First panel**, β-HA (lanes 1, 3) or His (lanes 2, 4) PD and IB for β and ζ (1 of 2 experiments). **Second panel**, x̄±SEM of ζ/β_2, n=2, unpaired *t*-test $p<0.05$. **Third panel**, pErk IB: 1 of 2 experiments. **Fourth panel**, x̄±SEM of pErk, n=2, unpaired *t*-test $p<0.0001$. **F** J76 wtc51 were lysed, incubated or not with sm-9V-A2 and subjected to PD by anti-HA or Talon beads. **Left**, β-HA (lanes 1, 3) or His (lanes 2, 4) PD and IB for β and ζ (1 of 5 experiments). **Right**, x̄±SD of ζ/β_2, n=5, unpaired *t*-test $p<0.0001$.